Tuning the Redox Potentials of Dinuclear Tungsten Oxo Complexes $[(Cp^*W(4,4'\text{-R,R-}2,2'\text{-bpy})(\mu\text{-O}))_2][PF_6]_2$ Toward Photochemical Water Splitting

Christian Cremer[a] and Peter Burger*[a,b]

Dedicated to Professor Richard A. Andersen on the occasion of his 60th birthday

Abstract: A series of novel dinuclear tungsten(IV) oxo complexes with disubstituted 4,4′-R,R-2,2′-bipyridyl (R_2bpy) ligands of the type $[(Cp^*W(R_2bpy)(\mu\text{-O}))_2][PF_6]_2$ ($R = NMe_2$, *t*Bu, Me, H, Cl) was prepared by hydrolysis of the tungsten(IV) trichloro complexes $[Cp^*W(R_2bpy)Cl_3]$. Cyclic voltammetry measurements for the tungsten(IV) oxo compounds provided evidence for one reversible oxidation and two reversible reductions leading to the oxidation states W^VW^{IV}, $W^{IV}W^{III}$ and $W^{III}W^{III}$. The corresponding complexes $[(Cp^*W(R_2bpy)(\mu\text{-O}))_2]^{n+}$ $[PF_6]_n$ ($n = 0$ for R = Me, *t*Bu, and 1, 3 for both R = Me) could be isolated after chemical oxidation/reduction of the tungsten(IV) oxo complexes. The crystal structures of the complexes $[(Cp^*W(R_2bpy)(\mu\text{-O}))_2][BPh_4]_2$ ($R = NMe_2$, *t*Bu) and $[(Cp^*W(Me_2bpy)(\mu\text{-O}))_2]^{n+}[PF_6]_n$ ($n =$ 0, 1, 2, 3) show a *cis* geometry with a puckered W_2O_2 four-membered ring for all compounds except $[(Cp^*W(Me_2bpy)(\mu\text{-O}))_2]$ which displays a *trans* geometry with a planar W_2O_2 ring. Examining the interaction of these novel tungsten oxo complexes with protons, we were able to show that the $W^{IV}W^{IV}$ complexes $[(Cp^*W(R_2bpy)(\mu\text{-O}))_2][PF_6^-]_2$ ($R = NMe_2$, *t*Bu) undergo reversible protonation, while the $W^{III}W^{III}$ complexes $[(Cp^*W(R_2bpy)(\mu\text{-O}))_2]$ transfer two electrons forming the $W^{IV}W^{IV}$ complex and molecular hydrogen.

Keywords: linear free energy relationships · N ligands · oxo ligands · redox chemistry · tungsten

Introduction

The chemistry of half-sandwich complexes of Group 6 metals in higher oxidation states is well developed and was recently reviewed by Poli.[1] His group has especially contributed to the research on Mo^{III-V} compounds,[2–6] while the groups of Green and Schrock have dedicated their work mainly to $W^{III,V,VI}$ compounds.[7–15] Interestingly, little is known about the chemistry of tungsten half-sandwich complexes in oxidation state IV and only few compounds of this type have been reported in recent years.[16–21] We recently reported a convenient entry into the chemistry of Cp* (η^5-$C_5Me_5^-$) tungsten(IV) complexes by means of one-electron reduction of the readily available starting material $[Cp^*WCl_4]$.[10, 22] We used this route to prepare a series of complexes of the type $[Cp^*W(R_2bpy)Cl_3]$, **1**-R, ($R = NMe_2$, *t*Bu, Me) with 4,4′-disubstituted 2,2′-bipyridyl (R_2bpy) donor ligands. Exploring the chemistry of these electron-rich tungsten(IV) complexes, we isolated the cationic $16e^-$ complexes $[Cp^*W(R_2bpy)Cl_2][BPh_4]$ and demonstrated that substituted bipyridine ligands can be used to tune the magnetic properties of these compounds.[23] Here we report the clean conversion of the trichloro complexes **1**-R into dinuclear tungsten(IV) oxo complexes of the type $[(Cp^*W(R_2bpy)(\mu\text{-O}))_2][PF_6]_2$, **3**-R, ($R = NMe_2$, *t*Bu, Me, H, Cl), which have remarkable spectroelectrochemical properties. Their reduction potentials can be tuned over a wide range using different R_2bpy ligands and their potential as novel systems for the photochemical splitting of water will be discussed.

[a] Prof. Dr. P. Burger, C. Cremer
Anorg.-chem. Institut
Universität Zürich, Winterthurerstrasse 190
8057 Zürich (Switzerland)
E-mail: chburger@aci.unizh.ch

[b] Present address:
Institut für Anorganische und Angewandte Chemie
Universität Hamburg
Martin-Luther-King Platz 6
20146 Hamburg
E-mail: burger@chemie.uni-hamburg.de

Results

Synthesis of tungsten(IV) oxo complexes 3-R: The series of tungsten oxo complexes **3**-R ($R = NMe_2$, *t*Bu, Me), was prepared from $[Cp^*WCl_4]$[10]. By in situ reduction of this complex with the mild reducing agent tetrakis(dimethylamino)ethylene (TDAE) in the presence of *para*-substituted bipyridine ligands (R_2bpy) the corresponding tungsten complexes $[Cp^*W(R_2bpy)Cl_3]$ **1**-R ($R = NMe_2$, *t*Bu, Me) were

 DOI: 10.1002/chem.200204330

obtained in excellent yields.[22] For the investigation of the electrochemistry of the oxo complexes **3**-R we intended to extend the series to the relatively electron poor ligands bpy and Cl_2bpy. However, due to the low solubility of the complexes **1**-H and **1**-Cl, we had to develop a different route to these compounds in high purity without insoluble by-products. As shown in Equation (1), the reaction of $[Cp^*WCl_2]_2$ with two equivalents bpy and Cl_2bpy at high temperatures led to the paramagnetic tungsten(III) complexes $[Cp^*W(R_2bpy)Cl_2]$, **2**-R, (R = H,[23] Cl).

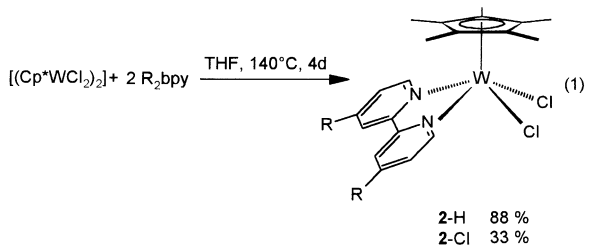

We reported earlier that complex **2**-H can be oxidized with $[Cp_2Fe][BPh_4]$ to the cationic tungsten(IV) complex $[Cp^*W(bpy)Cl_2][BPh_4]$.[23] According to Equation (2) the trichloro complexes **1**-H and **1**-Cl are accessible from **2**-R by oxidation with half an equivalent of hexachloroethane.

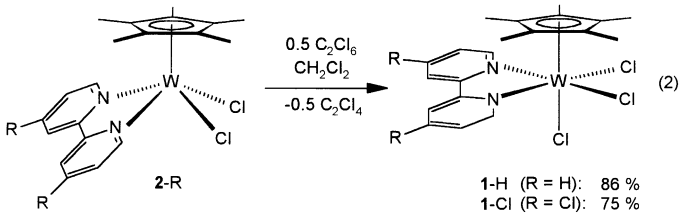

The dichloroethylene formed in this reaction can be easily removed in vacuo, or by washing with organic solvents, providing the analytically pure products in high yields.[24]

The complexes **1**-R readily dissolve in degassed water, forming deep red acidic (pH 1) solutions. After neutralization of the acid with $NaHCO_3$, the dimeric oxo bridged complexes $[(Cp^*W(R_2bpy)(\mu\text{-}O))_2][PF_6]_2$, **3**-R, were obtained in excellent yields by precipitation with NH_4PF_6 [Eq. (3)].

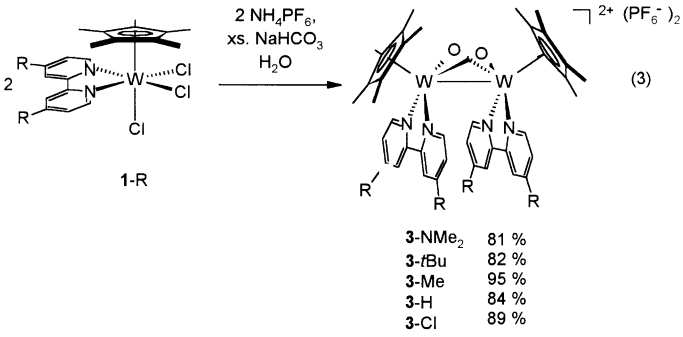

When water was present in low concentrations the hydrolysis was incomplete. This allowed us to isolate the dichloro oxo bridged complex $[(Cp^*W(Me_2bpy)(\mu\text{-}Cl))_2(\mu\text{-}O)]^{2+}$, **4**-Me, by hydrolysis of **1**-Me in non-dried organic solvents or by addition of stochiometric amounts of water to a THF solution.[22]

In addition, it was possible to obtain the water-soluble dimeric complex $[(Cp^*W(Me_2bpy)(\mu\text{-}O))_2]Cl_2$, $\mathbf{3}^{Cl}$-Me, from the hydrolysis of **1**-Me under basic conditions. The dimeric structures of the complexes **3**-NMe_2, **3**-*t*Bu and **3**-Me were unambiguously confirmed by X-ray crystal structure analysis (see below).

Crystal structures of complexes 3-Me, $\mathbf{3}^{BPh_4}$-*t*Bu and $\mathbf{3}^{BPh_4}$-$\mathbf{NMe_2}$: Single crystals suitable for structural analysis of the PF_6^- salts of **3**-R could only be obtained for complex **3**-Me. Since we were interested in the structural effect of different bipyridyl substituents, we prepared the BPh_4^- salts $\mathbf{3}^{BPh_4}$-*t*Bu and $\mathbf{3}^{BPh_4}$-NMe_2 by metathesis of **3**-*t*Bu and **3**-NMe_2 with $NaBPh_4$, from which we were able to grow single crystals. The crystal structures of the complexes are presented in Figures 1–3 and selected bond lengths and angles are given in Tables 1–3. Table 4 gives the data collection parameters used.

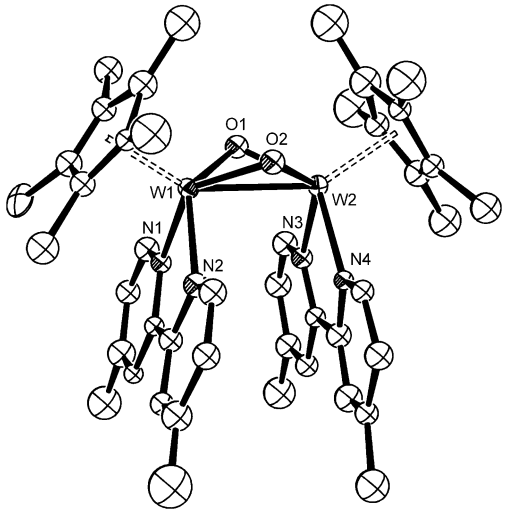

Figure 1. Molecular structure of complex **3**-Me; the anions are not shown (thermal ellipsoids at the 50% probability level).

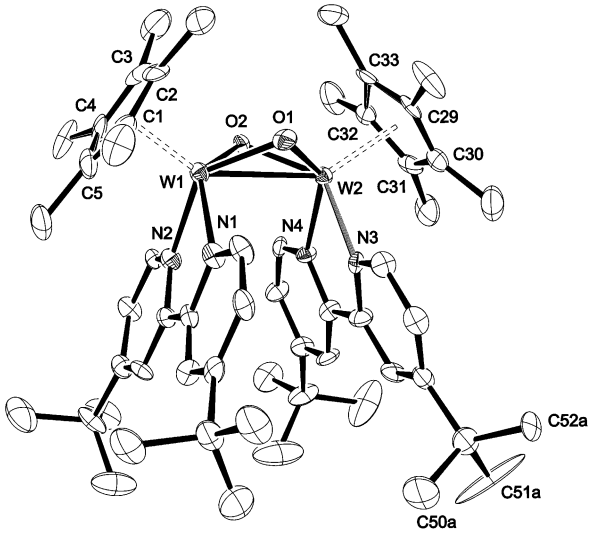

Figure 2. Molecular structure of complex $\mathbf{3}^{BPh_4}$-*t*Bu. Only one of the disordered positions of atoms C50a–C52a is shown; the anions have been omitted (thermal ellipsoids at the 50% probability level).

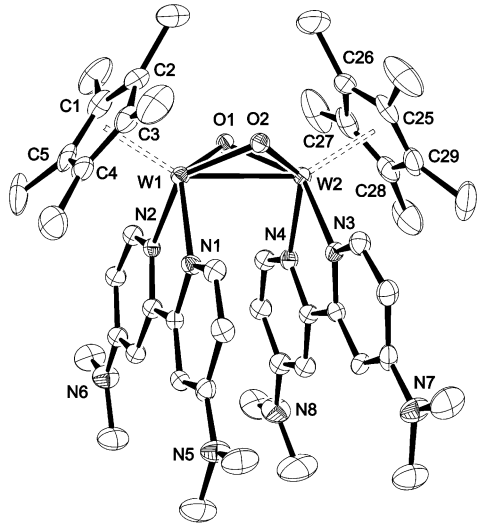

Figure 3. Molecular structure of complex 3^{BPh_4}-NMe_2; the anions are not shown (thermal ellipsoids at the 50% probability level).

Table 1. Selected bond lengths [Å] and angles [°] with estimated standard deviations (e.s.d.) for complex **3**-Me.

W1–O1	1.94(2)	W2–O1	1.93(2)
W1–O2	1.93(2)	W2–O2	1.93(2)
W1–N1	2.17(1)	W1–W2	2.7325(2)
W1–N2	2.18(1)	W1–Z1[a]	2.03
W1-O1-W2	90.9(5)	N1-W1-N2	74.2(7)
O1-W1-O2	76.4(6)	Z1-W1-O1	114.5
O1-W1-N1	87.9(7)	Z1-W1-O2	114.6
O1-W1-N2	135.4(7)	Z1-W1-N1	110.8
O2-W1-N1	134.5(7)	Z1-W1-N2	110.0
O2-W1-N2	87.5(7)	Z1-W1-W2	148.0

[a] Z1 is the ring centroid of carbon atoms C1–C5.

Table 2. Selected bond lengths [Å] and angles [°] with e.s.d. values for complex 3^{BPh_4}-NMe_2.

W1–O1	1.946(2)	W1–Z1[a]	2.02
W1–O2	1.960(2)	W1–C(Cp*)$_{gem}$	2.353
W1–N1	2.132(2)	W1–W2	2.7222(7)
W1–N2	2.158(2)		
W1-O1-W2	88.5(1)	N1-W1-N2	73.0(1)
W1-O2-W2	88.6(1)	N1-W1-W2	91.6(1)
O1-W1-O2	76.6(1)	N2-W1-W2	96.2(1)
O1-W1-W2	45.9(1)	Z1-W1-O1	117.3
O2-W1-W2	45.6(1)	Z1-W1-O2	111.9
O1-W1-N1	130.1(1)	Z1-W1-N1	112.2
O1-W1-N2	85.5(1)	Z1-W1-N2	109.4
O2-W1-N1	90.5(1)	Z1-W1-W2	148.9
O2-W1-N2	138.6(1)		

[a] Z1 is the ring centroid of carbon atoms C1–C5.

As can be seen from Figures 1–3, all three complexes **3**-R display a dimeric four-legged piano stool structure in which the monomers are linked by two bridging oxygen ligands. The Cp* ligands are arranged in a *cis* orientation, which leads to a close, nearly coplanar arrangement of the bipyridine ligands. The closest distances between the carbon atoms in the two bipyridine rings in complex **3**-Me are in the range 3.0–3.4 Å,

Table 3. Selected bond lengths [Å] and angles [°] with e.s.d. values for complex 3^{BPh_4}-*t*Bu.

W1–O1	1.952(4)	W1–Z1[a]	2.03
W1–O2	1.939(3)	W1–C(Cp*)$_{gem}$	2.359(6)
W1–N1	2.151(4)	W1–W2	2.7393(4)
W1–N2	2.159(4)		
W1-O1-W2	89.0(2)	N1-W1-N2	73.5(2)
W1-O2-W2	89.5(2)	N1-W1-W2	94.6(1)
O1-W1-O2	77.3(2)	N2-W1-W2	94.6(1)
O1-W1-W2	45.6(1)	Z1-W1-O1	113.2
O2-W1-W2	45.5(1)	Z1-W1-O2	111.8
O1-W1-N1	85.6(2)	Z1-W1-N1	112.3
O1-W1-N2	133.7(2)	Z1-W1-N2	112.9
O2-W1-N2	89.6(2)	Z1-W1-W2	145.5
O2-W1-N1	135.9(2)		

[a] Z1 is the ring centroid of carbon atoms C1–C5.

which is comparable to the distance between the layers in graphite (3.35 Å). The tungsten–tungsten distances of 2.7222(7), 2.7325(2) and 2.7393(4) Å for 3^{BPh_4}-NMe_2, **3**-Me and 3^{BPh_4}-*t*Bu, respectively, are in the range typical for tungsten–tungsten double bonds (see Discussion). The bond lengths and angles of the square pyramidal coordination spheres and of the puckered W_2O_2 ring are essentially identical in all three structures. The structural effects of the different bipyridine substituents are illustrated in Figure 4.

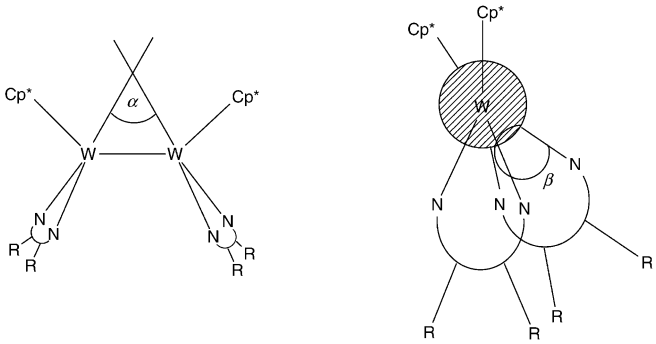

Figure 4. Structural effects of the bipyridine substituents and definitions of angles α and β.

The bulky *t*Bu substituents in complex 3^{BPh_4}-*t*Bu led to an increase of the angle α to 35.6°, which is about twice the value observed in 3^{BPh_4}-NMe_2 (13.6°) and **3**-Me (17.8°). In contrast to this, the dimethylamino substituents in complex 3^{BPh_4}-NMe_2 induce a twist between the two monomers, which is best seen by comparison of the angle β (Figure 4). This is just 1° for **3**-Me and 5° for 3^{BPh_4}-*t*Bu but is increased to 12° in 3^{BPh_4}-NMe_2.

Electrochemistry: Cyclic voltammograms for the complexes $[(Cp^*W(R_2bpy)(\mu\text{-}O))_2][PF_6]_2$, **3**-R, (R = NMe_2, Me, H, Cl) were recorded in acetonitrile in the range of +500 to −2500 mV and were referenced to the $[Cp_2Fe]/[Cp_2Fe^+]$ couple. The redox potentials $E_{1/2}$ and additional data (ΔE_p, I_{pc}/I_{pa}) are listed in Table 5; the cyclic voltammograms are shown in Figure 5.

Three reversible (quasi-reversible for **3**-Me) one-electron transfer steps II, III and IV were observed for all complexes and a fourth irreversible redox process I with a peak potential

Table 4. Data collection parameters of complexes **3**-Me, $\mathbf{3}^{BPh_4}$-*t*Bu and $\mathbf{3}^{BPh_4}$-NMe_2.

	3-Me	$\mathbf{3}^{BPh_4}$-*t*Bu	$\mathbf{3}^{BPh_4}$-NMe_2
formula	$C_{44}H_{54}F_{12}N_4O_2P_2W_2 \cdot 2$ acetone	$C_{104}H_{118}B_2N_4O_2W_2 \cdot 3CH_2Cl_2$	$C_{96}H_{106}B_2N_8O_2W_2 \cdot Et_2O \cdot$ acetone
F_w	1444.7	2100.2	2089.7
habitus	blue plate	blue rect. parallelepiped	green rect. parallelepiped
crystal dimension [mm]	$0.2 \times 0.1 \times 0.1$	$0.2 \times 0.15 \times 0.2$	$0.2 \times 0.3 \times 0.2$
crystal system	orthorhombic	orthorhombic	triclinic
space group	$P2_12_12_1$ (No 19)	*Pbca* (No 61)	$P\bar{1}$ (No 2)
a [Å]	10.734 (2)	27.394(1)	17.405(2)
b [Å]	17.879 (4)	23.820(1)	17.612(2)
c [Å]	28.067 (5)	29.818(2)	19.444(2)
α [°]			108.32(1)
β [°]			105.40(1)
γ [°]			108.09(1)
V [Å^3]	5386.4(2)	19457.0(17)	4923.7(9)
Z	4	8	2
ρ_{calcd} [g cm^{-3}]	1.782	1.428	1.374
μ [mm^{-1}]	1.6	2.58	2.39
$F(000)$	2848	8488	2090
T [K]	173	183(2)	183(2)
2θ [°]	4 – 58	4 – 45	4 – 52
no. of measured reflections (total unique)	7888, 7433	11236, 8031	17769, 13523
no. parameters	339	1150	1126
R_1 ($F^2 < 2\sigma F^2$)	0.0741	0.0280	0.0204
wR_2 ($F^2 < 2\sigma F^2$)	0.1924	0.0550	0.0362
GoF, S	1.01	1.233	1.169
res. el. dens. [e$^-$ Å^3]	1.74, – 1.59	0.78, – 0.78	0.62, – 0.62

Table 5. Results of cyclic voltammetry experiments for complexes **3**-R.

	$E_{1/2}$(I) [mV] (ΔE_p [mV], I_{pc}/I_{pa})	$E_{1/2}$(II) [mV] (ΔE_p [mV], I_{pc}/I_{pa})	$E_{1/2}$(III) [mV] (ΔE_p [mV], I_{pc}/I_{pa})	$E_{1/2}$(IV) [mV] (ΔE_p [mV], I_{pc}/I_{pa})
3-NMe_2	311[a]	– 734 (58, 1.12)	– 1999 (70, 1.84)	– 2252 (78, 1.00)
3-Me	–	– 243 (135, 0.68)	– 1387 (142, 1.37)	– 1775 (143, 3.71)
3-H	–	– 251 (88, 1.00)	– 1397 (80, 1.08)	– 1765 (90, 1.18)
3-Cl	–	– 116 (144, 0.96)	– 1232 (72, 1.22)	– 1414 (68, 0.97)

[a] Reported as E_{PA}.

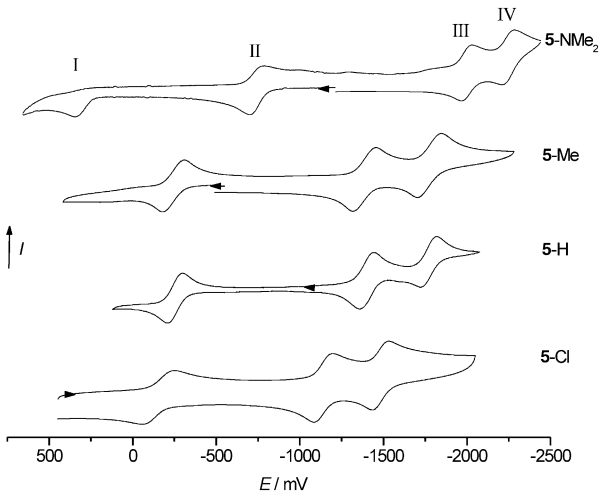

Figure 5. Cyclic voltammograms for complexes **5**-NMe_2, **5**-Me, **5**-H and **5**-Cl in CH_3CN vs $[Cp_2Fe]/[Cp_2Fe^+]$ at a scan rate of 200 mV s^{-1}, glassy carbon electrode (Pt for **5**-H) in 0.1 M NBu_4PF_6 solution.

of $E_{pa} = +311$ mV was observed for complex **3**-NMe_2. For complex **3**-Me the peak potentials ΔE_p are separated by approximately 140 mV and the I_{pc}/I_{pa} ratios were found to deviate more strongly from unity than for the other complexes. Nevertheless the cyclic voltammograms of **3**-Me did not change in repetitive scans (up to 10 scan cycles) and a plot of ln(I_{pc}) vs ln(scan speed) showed a linear correlation with a slope of 0.5, confirming the chemical reversibility of the redox processes. While a glassy carbon working electrode was applied for complexes **3**-NMe_2, **3**-Me and **3**-Cl. Satisfying data with $\Delta E_p < 100$ mV and $I_{pc}/I_{pa} \approx 1$ for **3**-H could only be obtained using a Pt electrode. Compared to the potentials observed at a glassy carbon electrode, the shift of the potentials for **3**-H at the Pt electrode are in the range of just 20 mV, which allowed us to compare the redox potential data of **3**-H and the other complexes.

For the water soluble chloride salt $[(Cp^*W(Me_2bpy)(\mu\text{-}O))_2]Cl_2$, $\mathbf{3}^{Cl}$-Me, a cyclic voltammogram was recorded in water using a glassy carbon working electrode and a Ag/AgCl reference electrode in the range +700 to – 1700 mV. A reversible redox couple was observed at – 155 mV ($\Delta E_p =$ 62 mV, $I_{pc}/I_{pa} = 0.64$) and two irreversible reduction waves appeared at $E_{pc} = -1177$ and – 1303 mV (measured at 10^{-3} M, not measured at constant pH).

For the non-aqueous measurements, plots of the redox potentials $E_{1/2}$ vs $4\sigma_p$[25] (for the four substituents R of the two bipyridine ligand) were found to display an excellent linear dependence on the correlation coefficients $R^2 = 0.97$, 0.97 and

0.99 (Figure 6). The derived reaction constants ρ for the redox couples II, III and IV, respectively, are $\rho = 180$, 223 and 231 mV. We decided to use the sum of the Hammett parameters $4\sigma_p$ for the correlation to allow a comparison of

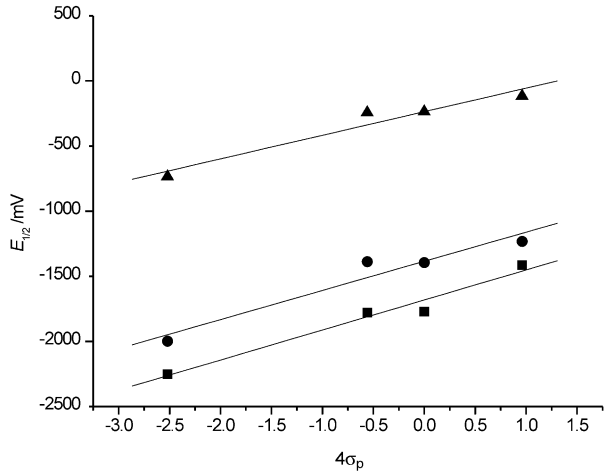

Figure 6. Hammett correlations for the half-wave potentials $E_{1/2}$(II) (▲), $E_{1/2}$(III) (●) and $E_{1/2}$(IV) (■) for complexes **3**-NMe_2, **3**-Me, **3**-H and **3**-Cl.

the reaction constants ρ with previously studied systems. This method has been widely applied in polysubstituted systems.[26–29] As Jordan et al. demonstrated for the stepwise bromo substitution of metalloporphyrins, however, substituent effects on reduction potentials are not necessarily additive.[30]

Isolation of the electrochemically observed species: In order to assess the oxidation states of the electrochemically generated redox couples of the complexes **3**-R, we intended to isolate the corresponding species by chemical oxidation/reduction of complex **3**-Me. For the latter compound, the oxidation wave (II) was observed at $E_{1/2} = -242$ mV vs the $[Cp_2Fe]/[Cp_2Fe^+]$ couple. Indeed, chemical oxidation of **3**-Me with one equivalent of ferrocinium hexafluorophosphate resulted in an immediate color change from blue to red upon addition of the oxidizing agent [Eq. (4)].

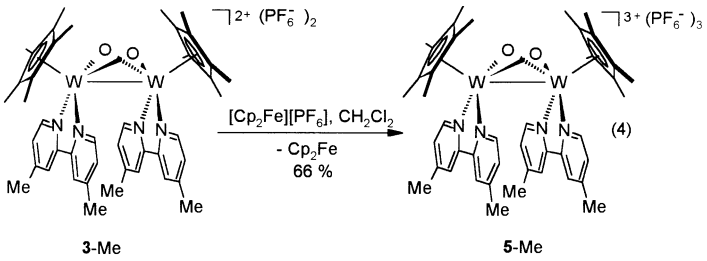

From the reaction mixture, the tricationic paramagnetic complex $[(Cp^*W(Me_2bpy)(\mu\text{-}O))_2][PF_6]_3$, **5**-Me, was isolated and the dimeric structure was confirmed by an X-ray crystal structure analysis (cf. next Section). This result allowed us to assign the half-wave potential II to the redox couple $W^VW^{IV}/W^{IV}W^{IV}$ and the potentials III and IV to the redox couples $W^{IV}W^{IV}/W^{IV}W^{III}$ and $W^{IV}W^{III}/W^{III}W^{III}$, respectively.

To achieve both reduction steps, we reacted complexes **3**-Me and **3**-*t*Bu with two equivalents of sodium naphthalenide according to Equation (5).

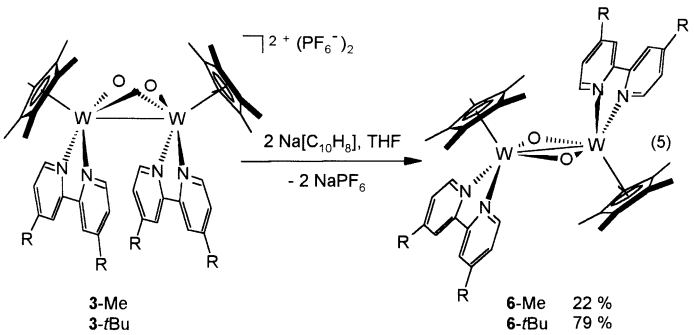

From the resulting deep violet reaction mixtures, the diamagnetic complexes $[(Cp^*W(R_2bpy)(\mu\text{-}O))_2]$, **6**-Me and **6**-*t*Bu, were isolated. The diamagnetism of the two complexes indicated a dimeric structure with antiferromagnetically coupled W^{III} metal centers, which was unambiguously confirmed by the X-ray crystal structure of **6**-Me (see below).

The mixed valence mono cationic complex $[(Cp^*W(Me_2bpy)(\mu\text{-}O))_2][PF_6]$, **7**-Me, was isolated as a side product of the reduction process of **3**-Me to **6**-Me, which allowed us to determine the crystal structure of this compound (see next Section). Unfortunately, further attempts to prepare this complex by one-electron reduction of **3**-Me or by one-electron oxidation of **6**-Me failed.

To get further information about the interaction between the metal centers in the system $[(Cp^*W(R_2bpy)(\mu\text{-}O))_2]^{n+}$, the comproportionation constants K_{comp} for the mixed valence species **7**-R were determined from the half-wave potentials $E_{1/2}$(III) and $E_{1/2}$(IV) using the relation $\log(K_{comp}) = 16.9(E_{1/2}(III) - E_{1/2}(IV))$.[31] The derived values of $K_{comp} = 10^3$ (R = Cl), 2×10^4 (R = NMe_2), 2×10^6 (R = H) and 4×10^6 (R = Me) are between the typical ranges for class II (partially localized valence electrons) and class III (delocalized valence electrons) mixed valence complexes in the classification of Robin and Day (see discussion).[32]

Structural analysis of complexes 5-Me, 6-Me and 7-Me: To examine the influence of the oxidation states on the structure of the dimeric tungsten oxo complexes, we studied the crystal structures of **5**-Me, **6**-Me and **7**-Me by single crystal X-ray diffraction. The molecular structures are shown in Figures 7–9, and selected bonds and angles are presented in Tables 6–8.

Figures 7–9 clearly show that the dimeric four-legged piano stool structure established for complexes **3**-R is also maintained in **5**-Me, **6**-Me and **7**-Me. Complexes **7**-Me and **5**-Me show a strong resemblance to the structure observed for **3**-Me, showing no significant changes in the bond lengths and angles. Notably, the metal-metal distances are in the narrow range of 2.6869(5) Å for **5**-Me and 2.7582(3) Å for **6**-Me, which experience just a slight increase of 2% with decreasing oxidation states.

Complex **6**-Me on the other hand, differs from all other structures presented in this work and displays a *trans*

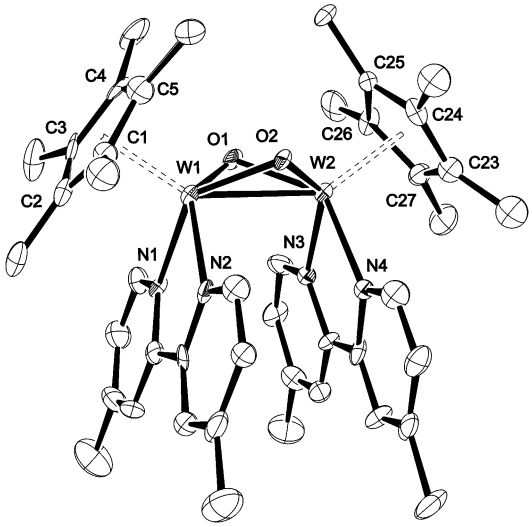

Figure 7. Molecular structure of complex **5**-Me; the anions are not shown (thermal ellipsoids at the 50% probability level).

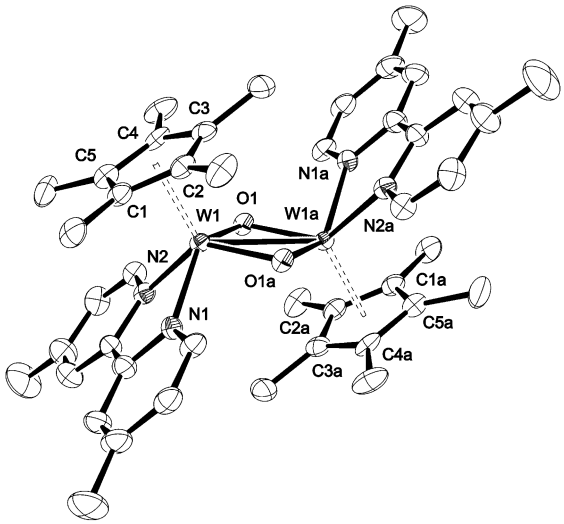

Figure 8. Molecular structure of complex **6**-Me (thermal ellipsoids at the 50% probability level).

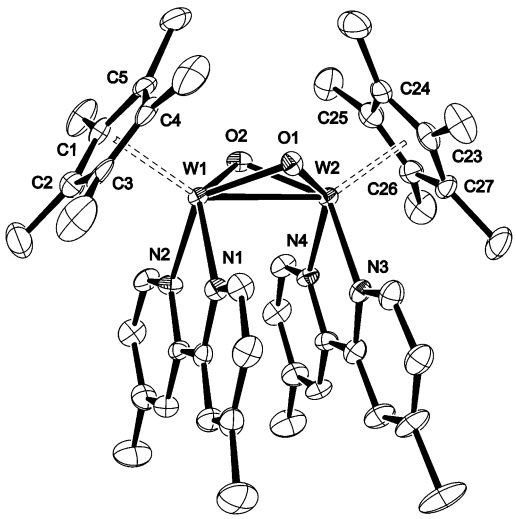

Figure 9. Molecular structure of complex **7**-Me; the anion is not shown (thermal ellipsoids at the 50% probability level).

Table 6. Selected bond lengths [Å] and angles [°] with e.s.d. values for complex **5**-Me.

W1–O1	1.921(5)	W1–Z1[a]	2.06
W1–O2	1.9382(6)	W1–C(Cp*)$_{av}$	2.39(1)
W1–N1	2.174(5)	W1–W2	2.6869(5)
W1–N2	2.161(6)		
W1-O1-W2	87.6(2)	N1-W1-N2	73.1(2)
W1-O2-W2	88.6(2)	N1-W1-W2	95.5(2)
O1-W1-O2	79.5(2)	N2-W1-W2	95.7(2)
O1-W1-W2	46.3(1)	Z1-W1-O1	113.2
O2-W1-W2	45.8(1)	Z1-W1-O2	114.1
O1-W1-N1	87.7(2)	Z1-W1-N1	110.9
O1-W1-N2	136.2(2)	Z1-W1-N2	110.4
O2-W1-N1	134.6(2)	Z1-W1-W2	147.0
O2-W1-N2	86.5(2)		

[a] Z1 is the ring centroid of carbon atoms C1 – C5.

Table 7. Selected bond lengths [Å] and angles [°] with e.s.d. values for complex **7**-Me.

W1–O1	1.963(3)	W1–Z1[a]	2.04
W1–O2	1.965(4)	W1–C(Cp*)$_{av}$	2.371(6)
W1–N1	2.151(4)	W1–W2	2.7404(3)
W1–N2	2.135(4)		
W1-O1-W2	88.7(1)	N1-W1-N2	73.4(1)
W1-O2-W2	88.8(2)	N1-W1-W2	94.7(1)
O1-W1-O2	77.8(2)	N2-W1-W2	91.9(1)
O1-W1-W2	45.5(1)	Z1-W1-O1	115.3
O2-W1-W2	45.4(1)	Z1-W1-O2	113.0
O1-W1-N1	85.5(2)	Z1-W1-N1	111.6
O1-W1-N2	131.0(2)	Z1-W1-N2	113.5
O2-W1-N1	135.4(2)	Z1-W1-W2	147.3
O2-W1-N2	87.1(2)		

[a] Z1 is the ring centroid of carbon atoms C1 – C5.

Table 8. Selected bond lengths [Å] and angles [°] with e.s.d. values for complex **6**-Me.

W1–O1	1.971(3)	W1–Z1[a]	2.07
W1–O1a	1.976(3)	W–C(Cp*)$_{av}$	2.395(4)
W1–N1	2.086(3)	W1–W1a	2.7582(3)
W1–N2	2.081(4)		
W1-O1-W2	88.7(1)	N1-W1-N2	72.7(1)
O1-W1-O1a	91.3(1)	N1-W1-W1a	113.8(1)
O1-W1-W1a	45.7(1)	N2-W1-W1a	113.0(1)
O1-W1a-W1	45.6(1)	Z1-W1-O1	111.6
O1-W1-N1	135.1(1)	Z1-W1-O1a	111.6
O1-W1-N2	81.4(1)	Z1-W1-N1	112.2
O1a-W1-N1	81.8(1)	Z1-W1-N2	113.3
O1a-W1-N2	134.0(1)	Z1-W1-W1a	121.8

[a] Z1 is the ring centroid of carbon atoms C1 – C5.

arrangement of the Cp* ligands with a flat (unpuckered) W_2O_2 ring. As a consequence, the O-W-O angle is larger (91.3(1)°) and the Z-W-W angle smaller (121.8°) compared to the structures of complexes **3**-R, **5**-Me and **7**-Me (average of 77° for O-W-O and 147° for Z-W-W).

Proton reduction by [Cp*W(R$_2$bpy)(μ-O)]$_2$, 6-R: To test whether the lower valent $W^{III}W^{III}$ complex **6**-*t*Bu would allow the reduction of H^+ to H_2, we examined the reaction of **6**-*t*Bu with two equivalents of HOTf in [D$_8$]THF contained in a Teflon-tap-sealed NMR tube [Eq. (6)].

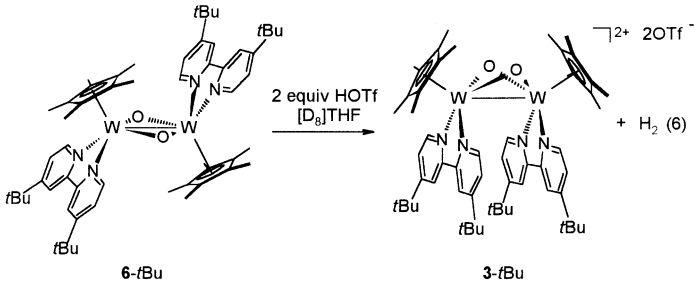

Upon addition of the acid, an immediate color change of the solution from violet to blue occurred and a black precipitate formed. The ^{1}H NMR spectrum of the reaction mixture showed small amounts of the protonated complex, $[(Cp^*W(t\mathrm{Bu}_2\mathrm{bpy})(\mu\text{-}O)(\mu\text{-}OH)](OTf)_3$, **8**-*t*Bu, and a singlet at $\delta = 4.55$ that was assigned to hydrogen after comparison with a reference sample. The same proton resonance was found in the solvent after vacuum transfer. The precipitate was isolated and identified by ^{1}H and ^{19}F NMR spectroscopy as the triflate salt of complex **3**-*t*Bu with a yield of 60%.

It is noteworthy that we were not able to detect intermediates in the reaction of complexes **6**-R with acid, even when the reaction of the soluble acid $[HB(C_6H_3(CF_3)_2)_4 \cdot 2Et_2O]$ was monitored by NMR spectroscopy at low temperatures. In order to find out how these dimeric complexes interact with protons, the reaction of the higher valent $W^{IV}W^{IV}$ complexes **3**-R (R = Me, *t*Bu, NMe_2) with HOTf was examined [Eq. (7)].

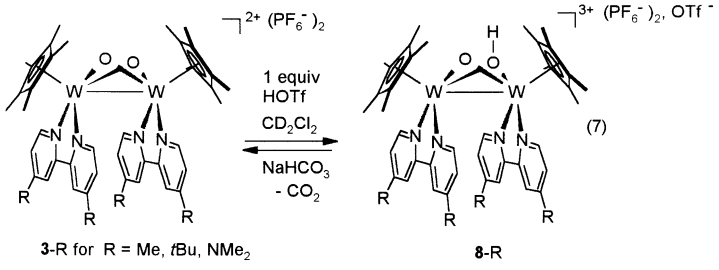

When one equivalent HOTf was added to a CD_2Cl_2 solution of these complexes, the color changed immediately from blue to red (green for **3**-NMe_2). In the ^{1}H NMR spectra, two sets of resonances were observed for the diasterotopic protons of the bpy ligands and a broad singlet for an (acidic) proton was observed between $\delta = 10$ and 12. Notably, when a second equivalent of HOTf was added, the resonances of the protonated complexes and in addition, the resonance of free HOTf was detected. We take this as a strong hint that the complexes are *not* protonated twice. After addition of $NaHCO_3$ to the NMR samples the complexes **3**-R were completely regenerated. For the methyl derivative **3**-Me, we were able to isolate and fully characterize its protonated congener, complex $[(Cp^*W(Me_2bpy)(\mu\text{-}OH)(\mu\text{-}O)][PF_6]_2][OTf]$, **8**-Me. Complex **8**-Me is stable in the solid state but in CD_2Cl_2 solution traces of $[(Cp^*W(Me_2bpy)(\mu\text{-}O))_2][PF_6]_2$, **3**-Me, were observed in the ^{1}H NMR spectrum after several hours. For the ^{13}C NMR characterization, this was prevented by addition of a small amount of HOTf to the NMR solution. Both, the ^{1}H and ^{13}C NMR spectra of **8**-Me show two sets of resonances for each ring of the Me_2bpy ligand but only one set for the two Cp* ligands. The ^{19}F NMR spectrum displays resonances in the ratio 4:1 for two PF_6^- and one OTf^- counter ion.

The downfield shift of the resonance in the range of $\delta = 10-12$ and the absence of tungsten satellites of the signal provide evidence against protonation at one of the metal centers. Since protonation at the bpy nitrogen atoms or one of the metal centers would lead to an inequivalence of the Cp* ligands, these data provide support for the protonation at one of the bridging oxygen ligands leading to the proposed structure shown for complexes **8**-R in Equation (7). Further evidence for protonation at one of the oxygen bridges was provided by a crystal structure analysis of **8**-Me. Although we had problems with the refinement due to positional disorder of the PF_6^- and OTf^- anions, it clearly revealed a dimeric μ-oxo bridged structure with slightly different W–O lengths of the two bridging oxygen ligands.[33]

Protonation is also possible in water and was established for the water soluble complex $\mathbf{3}^{Cl}$-Me. When the pH changes upon addition of concentrated HCl to a diluted aqueous solution of $\mathbf{3}^{Cl}$-Me ($c = 10^{-4}$ M) were recorded, a well-defined color change from blue to red was observed between pH 0.8 and 1.5. It is noteworthy that the UV spectrum of this red solution was identical to the spectrum of **8**-Me in methylenechloride.

Discussion

X-ray crystal structures of $[(Cp^*W(R_2bpy)(\mu\text{-}O))_2]^{n+}$, 3-R, 5-Me, 6-Me, 7-Me: All six structurally characterized complexes of the type $[(Cp^*W(R_2bpy)(\mu\text{-}O))_2]^{n+}$ ($n = 3$ (**5**-Me), $n = 2$ (**3**-R), $n = 1$ (**7**-Me), $n = 0$ (**6**-Me, **6**-*t*Bu)) display a dimeric piano stool geometry with two μ-O-bridging ligands, L. This is a common structural motif for high-valent transition metal complexes of V, Cr, Mo, W, Re, Fe, Co,[34, 35] and as observed in this work, both puckered and flat M_2L_2 rings are known.[36–39] The metal–ligand bond lengths in the six structures vary only over a small range, with average W–(μ-O) lengths from 1.93 (**5**-Me) to 1.97 Å (**6**-Me), average W–N lengths from 2.08 (**6**-Me) to 2.17 Å (**5**-Me) and W–Z lengths from 2.02 (3^{BPh_4}-NMe_2) to 2.07 Å (**6**-Me). It is noteworthy that compared to compiled metal–ligand bond lengths for tungsten and molybdenum complexes the W–(μ-O) bonds are rather long, whereas the W–N bonds are rather short.[40] We attribute this to relatively electron rich metal centers in the dimeric oxo bridged system $[(Cp^*W(R_2bpy)(\mu\text{-}O))_2]^{n+}$, which is presumed to lead to stronger bonding to the bipyridine π acceptor and weaker bonding to the oxo donor ligands. This is consistent with the finding that the longest W–(μ-O) and shortest W–N bonds in the series were observed for the reduced $W^{III}W^{III}$ complex **6**-Me. The rather long W–(μ-O) bonds also indicate that π-donation of the oxo ligands is negligible and, hence, they can be considered as two-electron donors in these systems.

With the exception of complex **6**-Me, the bond angles around the metal centers are also essentially identical, with small variations of 1–7%. The O-W-O angle of the W_2O_2 ring

of 91.3(1)° in **6**-Me compares with an average of 77.4° in the structures with a *cis* geometry, which is presumably due to the planar arrangement of the W_2O_2 ring in **6**-Me and the puckered rings in the other structures. Another feature of **6**-Me is the more acute Z-W-W angle of 121.8° compared to 146–147° in the *cis* complexes. This is probably a consequence of the steric repulsion between the Cp* ligands in the *cis* geometry, which is best seen from the short interannular Cp* methyl carbon distances of 3.60 Å.

In the *cis*-oriented complexes, a close coplanar arrangement of the bipyridine ligands is observed. This is deemed a consequence of the sterically crowded ligand sphere of the formally 8-coordinate metal centers. In complex **3**-Me, for example, the distances between the two bipyridine ligands are in the range of 3.0–3.4 Å, which is comparable to the distance between the layers in graphite (3.35 Å). Therefore, we expected that a change in the steric demand of the bipyridine substituents could have a strong structural influence. As can be seen from Figure 4, however, even for complex **3**-*t*Bu with the bulky *t*Bu groups, only small geometrical changes could be observed. In the latter, widening of the angle between the bipyridyl ligands to 35.6° occurred, which is about twice the value observed for **3**-Me. For **3**-NMe_2 with the "flat" dimethylamino groups on the other hand, a twist of the two halves of the complex by 12° was determined (Figure 4).

Based on electron counting rules and considering the μ-oxo ligands as two-electron donors (see above), one would expect metal–metal bond orders of 1.0 for complex **6**-R, 1.5 for **7**-Me and **5**-Me and 2.0 for **3**-R. This, however, is not reflected in the crystallographically determined W–W separations, which display only a slight increase in the order **5**-Me (2.6869(5) Å) < **3**-R (2.73 Å (average)) < **7**-Me (2.7404(3) Å) < **6**-Me (2.7582(3) Å). This rather small change of 2–3% can be explained by an increased repulsion between filled metal d orbitals with decreasing oxidation state. This observation is in agreement with previous reports on related halo-[41, 42] and sulfur-bridged[43] dimeric piano stool complexes of molybdenum, which also displayed small effects of the oxidation states of the transition metal on the M–M separation. The authors therefore concluded that the metal–metal distance depends rather on the number and type of bridging ligands. This can be illustrated by the large differences found for the formal M–M double bonds in $[(CpMo(\mu\text{-}O)(\mu\text{-}S)(\mu\text{-}SMe))_2]$[43] (2.4900(3) Å) and $[(Cp^*Mo(S)(\mu\text{-}S))_2]$[44] (2.905(1) Å). In this regard, it deserves a special mention that the formal W–W triple bond of 2.3678(6) Å observed in $[((C_5H_4iPr)WCl_2)_2]$[45] is significantly shorter than the M–M separation found in this work.

Complexes **3**-R display a remarkable stability of the dimeric μ-oxo-bridged structure even for the compounds with bulky substituents. The crystal structure of the molybdenum congener of **3**-Me, $[(Cp^*Mo(Me_2bpy)(\mu\text{-}O))_2][PF_6]_2$ is also noteworthy in this regard, since it also revealed a dimeric structure.[33] Though the dimeric structure of the complexes $[(Cp^*W(R_2bpy)(\mu\text{-}O))_2]^{n+}$ was proved unambiguously in the solid state, we considered dissociation of the dimers in solution. In particular, this was based on the monomeric structure observed in the X-ray crystal structure of the closely related molybdenum complex $[CpMo(dmpe)(=O)][PF_6]$.[46]

However, IR spectra of complexes **3**-R in dilute solutions revealed the absence of ν(W=O) bands in the 800–1000 cm^{-1} range[47] typical for terminal tungsten–oxygen double bonds, thus providing evidence against the presence of a monomeric $[Cp^*W(R_2bpy)(=O)]^+$ species. Further support that the dimeric structure is maintained in solution was obtained by the following crossover experiment: According to ^1H and ^{13}C NMR spectral analysis, hydrolysis of an 1:1 mixture of **1**-Me and **1**-*t*Bu led to a product mixture of three complexes in approximate 1:1:2 ratio, that is **3**-Me, **3**-*t*Bu and, the mixed dimer containing both a Me_2bpy and a tBu_2bpy ligand. This is consistent with a dimeric structure and allowed us to rule out dissociation into the monomers for which only two sets of resonances would have been expected.

Based on these results, we concluded that the type of ligand (dmpe instead of R_2bpy) was responsible for the preferred monomeric structure of $[CpMo(dmpe)(=O)][PF_6]$. This was supported by a comparative extended Hückel (EHT) analysis of the monomeric model systems $[CpWL_2(O)]^+$ with L_2=HN=CH–CH=NH and $(PH_3)_2$. As can be readily seen from inspection of Figure 10, one of the frontier orbitals in this system can be described as an essentially purely metal centered d_{z^2} orbital.

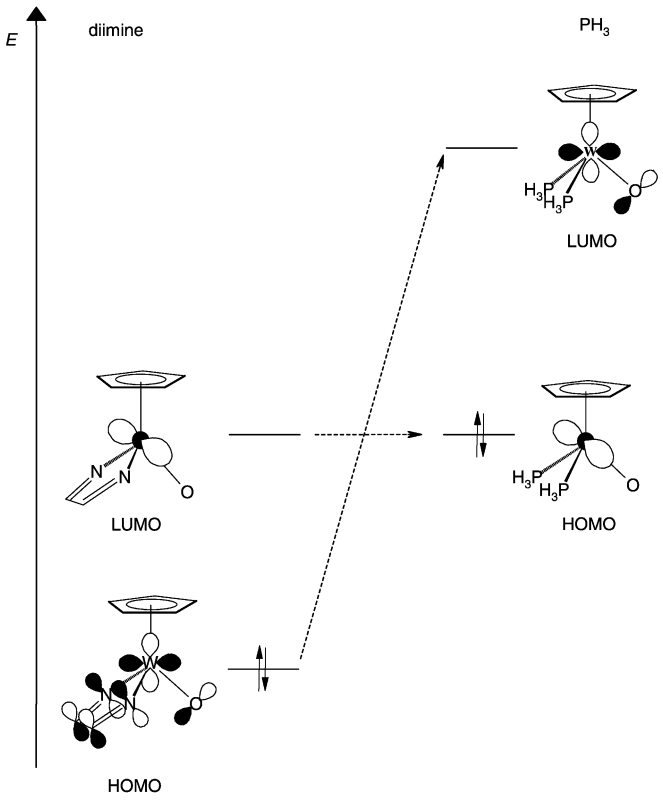

Figure 10. Frontier orbitals for the model system $[CpWL_2(O)]^+$ with L_2=HN=CH–CH=NH and $(PH_3)_2$.

The second frontier orbital is characterized by an antibonding interaction between a metal-based $d_{x^2-y^2}$ and an oxygen-based orbital. For the diimine ligand this interaction is strongly stabilized by mixing of a δ^* acceptor orbital of the diimine ligand. Due to the substantially weaker π acceptor

propensity of the phosphine ligands, the latter interaction is *significantly* reduced in $[CpW(PH_3)_2(O)]^+$, which eventually leads to *inversion* of the energy levels and, hence *different* population of the frontier orbitals in the model complexes. For L_2=HN=CH–CH=NH, the LUMO (d_{z^2} orbital) is therefore an ideal acceptor orbital for the bridging oxygen ligands in the dimeric complexes **3**-R. The latter is filled in the PH_3 complex and thus not available for bonding to the oxygen donors. Dimerization in the phosphine complex is disfavored due to a $4e^-$, two-orbital repulsive term, which provides an explanation for the observed structural preferences in the phosphine and bipyridine complexes.

Electrochemistry of the complexes 3-R: The cyclic voltammetry measurements for complexes **3**-R in combination with the isolation of the complexes **5**-Me, **6**-R and **7**-Me established that the compounds **3**-R undergo three electrochemically as well as chemically reversible one-electron transfer steps, that is one oxidation (II) and two reversible reduction processes (III, IV). For the more electron rich complex **3**-NMe_2 one further, albeit irreversible, oxidation wave (I) was observed. Presently it is unclear whether the irreversibility of the second oxidation step is due to deposition of the insoluble quadruply charged W^VW^V species on the electrode or to consecutive chemical reactions, for example fast coordination of acetonitrile to the Lewis-acidic metal centers, occurs.

The isolated complexes **7**-Me and **5**-Me display essentially identical geometrical parameters to complex **3**-Me. It is therefore anticipated that they correspond to the electrochemically generated species of the oxidation and the first reduction step. This is in contrast to the second reduction wave IV. While the latter is also an electrochemically reversible redox process, the crystal structure analysis of the independently prepared and isolated complex **5**-Me evidenced a *cis*–*trans* rearrangement during its preparation. At first glance, this might be indicative of an EC mechanism with a fast consecutive chemical rearrangement process. However, this could be ruled out by the cyclic voltammogram for the oxidation process of isolated **6**-Me, which was significantly distinguishable from the CV of **3**-Me. It is therefore deemed that the *cis*-geometry of **3**-Me is maintained on the timescale of the electrochemical experiment. This is supported by hold-ramp experiments and repetitive scans, which evidenced no change of the cyclic voltammogram. A bulk electrolysis experiment of **6**-*t*Bu (at -600 mV, consumption of ca. 1.7 e^- molecule^{-1}, duration ca. 2 h) confirmed nevertheless the reversibility of the *cis*–*trans* rearrangement process on the slower preparative time scale. In addition, oxidation of **6**-*t*Bu with triflic acid also led to the *cis*-configured complex **3**-*t*Bu [Eq. (6)].

Mechanistically, the rearrangement process is initiated by the electron transfer step IV. As presented in Scheme 1, it is anticipated to proceed by a breaking of the oxygen–tungsten bonds followed by 180° rotation about the metal–metal bond.

Based on the theoretically-supported mechanism for the *cis*–*trans* isomerization in $[(Cp^*MoS(\mu\text{-}S))_2]$, an alternative mechanism with *complete* dissociation to give $[Cp^*W(=O)(R_2bpy)]$ and consecutive reassociation of this transient is deemed less likely.[35]

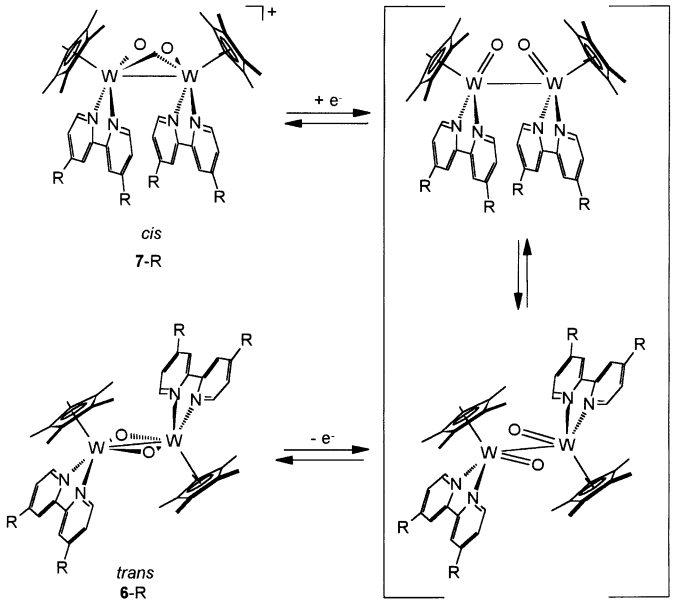

Scheme 1.

Comparison of the cyclic voltammograms in Figure 5 and the data in Table 5 clearly show that the bipyridine substituents R have a strong influence on the position of the redox potentials of complexes **3**-R; the more electron donating R substituents lead to a substantial shift of the potentials to lower values. This is nicely reflected in the linear correlation of the Hammett parameters for the substituents R and the measured potentials II, III and IV (Figure 6). The reaction constants obtained for Equation (8) of 180, 223 and 231 mV for the redox couples II, III and IV, respectively, are extraordinary high compared to values reported in related studies of mono and dinuclear systems, which are typically in the range 82–114 mV.[27–29, 48] Even for the relatively small range of Hammett parameters used, a systematic tuning over a range of approximatley 800 mV is thus possible. Note that this is among the largest shifts observed for a homologous series of transition metal complexes.[49]

$$\Delta E_{1/2} = E_{1/2}(R) - E_{1/2}(H) = \rho 4\sigma \quad (8)$$

Finally, it should be noted that the assigned formal oxidation states W^VW^{IV} and $W^{IV}W^{III}$ for the mixed valence complexes **5**-Me and **7**-Me do not display the real electron configurations, which are rather $d^{1.5}d^{1.5}$ and $d^{2.5}d^{2.5}$ than d^1d^2 and d^2d^3. The crystal structure analysis clearly indicated a metal–metal bond in both complexes (see next Section) and therefore delocalization of the valence electrons over the two metal centers. This was further supported by the values for the comproportionation constants K_{comp} for complexes **7**-R, which are in the range of 4×10^6 (R = Me) to 10^3 (R = Cl). According to Creutz et al. the value of K_{comp} can be used as a measure for the delocalization of valence electrons in dinuclear mixed valence complexes,[31] which were categorized by Robin and Day as class I, II and III for localized, partially localized and delocalized valence electrons.[32] The values for **7**-R are in the typical ranges for class II (20–500) and class III (10^6–10^{12}) compounds, therefore providing

evidence of rather delocalized valence electrons in these systems.

Potential for the photochemical water reduction: The remarkable reversible and tunable redox chemistry in combination with the structural stability the complexes **3**-R gives these compounds great potential as redox catalysts.

In particular, the water solubility and strong absorption coefficients (up to $\varepsilon = 10^4\,L\,mol^{-1}\,cm^{-1}$) in the visible spectrum up to 800 nm led us to consider complexes **3**-R as novel systems for the photochemical water splitting process.[50] A catalytic system has to meet several requirements, including suitable redox potentials (+0.82 to −0.41 V vs NHE), long-lived excited states and the ability to bind protons. Most of the known systems for the photochemical water splitting process are therefore multi component systems containing a photosensitizer with a long-lived excited state that provides an electron to electron relay. From there, the electron is further transferred to a redox catalyst such as finely dispersed Pt, which is able to reduce H^+ to H_2.

Probably the most extensively studied system is the photosensitizer $[Ru(bpy)_3]^{2+}$ in combination with methyl viologen as the electron relay and colloidal Pt as redox catalyst.[51] However, a major disadvantage of the Ru system is that it cannot be protonated, which is important for the reduction of H^+ to prevent the energetically unfavorable formation of H radicals. Therefore a cocatalyst such as Pt or complexes like $[(Cp^*M(PR_2))_2]$ (M = Co, Rh)[52] has to be used.

As shown in Equation (6) the reduced form of the complexes **3**-R are able to reduce protons to dihydrogen. The reversible protonation step of **3**-Me leading to the protonated compound **8**-Me [Eq. (7)] indicates a potential pathway for interaction between the complex and the proton.

Since complexes **3**-R strongly absorb light in the visible region of up to 800 nm (ε as high as $\varepsilon = 10^4\,L\,mol^{-1}\,cm^{-1}$) they might combine the role of a redox catalyst and photosensitizer. In preliminary irradiation experiments of aqueous solutions of **5**-Me at pH 7 and 1, however, we have not, so far, detected the formation of H_2. This might be explained by the absence of an excited state with a sufficiently long lifetime to allow electron transfer/protonation. It is noteworthy, however, that complexes **3**-R and **8**-Me display a strong fluorescence band when irradiated in the visible region. While this implies an accessible excited state with a sizable lifetime, the lifetime of the excited state is yet unknown. Since Constable et al. previously established that the substituents at the terpyridyl rings have a strong influence on the lifetime of excited states in $Ru(terpy)_2$ systems,[53] we hope to observe a similar correlation for the R_2bpy substituted complexes **3**-R in the future.

While the complexes **3**-R in the isolated reduced state (**6**-R) are able to reduce protons to hydrogen, the potential for the redox couple $W^{V}W^{IV}/W^{IV}W^{IV}$ is still too low for the oxidation of water to oxygen ($O^{2-} = O_2 + 2e^-$). The half-wave potential determined for $\mathbf{3}^{Cl}$-Me vs Ag/AgCl in water is $E_{1/2} = -0.154$ V (+0.04 V vs NHE), compared with the potential of $E^0 = +0.82$ V for the process $2H_2O = 4H^+ + O_2 + 4e^-$ at pH 7.[51] However, the results of the Hammett correlation show that the potential for the oxidation can be increased by 0.13 V going from Me_2bpy to Cl_2bpy. For the even more electron poor R_2bpy ligands with R = CF_3 or NO_2 substituents, one can estimate that a potential of +0.6 V should be accessible. We anticipate that the potential can be even further shifted to higher values for the analogous molybdenum compounds and are currently following this idea up.

Conclusion

In this work, synthetic access to a series of novel dimeric tungsten(IV) oxo complexes is described. These compounds display three fully reversible redox steps, which are strongly correlated with the *para* substituents of the bipyridine ligands. This allows us to tune the redox potentials over a wide range. In combination with the strong absorptions in the visible and NIR range, these systems are deemed to have a high potential as photochemical redox catalysts, in particular for the photochemical water splitting process. Further work directed to possible applications of these systems is currently in progress.

Experimental Section

General methods: Reactions were carried out under a N_2 atmosphere using glovebox and Schlenk techniques. The halogenated solvents were thoroughly dried over P_4O_{10} and saturated with N_2. The other solvents were distilled under nitrogen from violet sodium/benzophenone and stored under nitrogen. The deuterated solvents were dried over sodium or P_4O_{10} and transferred in vacuo using high-vacuum techniques. 2,2′-bipyridyl was purchased from Fluka and used as received. The compounds $[Cp_2Fe][BPh_4]$,[54] Cl_2bpy,[55] $[HB(C_6H_3(CF_3)_2)_4 \cdot 2\,Et_2O]$,[56] $[Cp^*W(R_2bpy)Cl_3]$, **1**-R, (R = Me, *t*Bu, NMe_2)[22] and $[Cp^*W(bpy)Cl_2]$, **2**-H,[23] were prepared following published methods. The dimeric complex $[(Cp^*WCl_2)_2]$[57] was obtained from $[Cp^*WCl_4]$[10] by a modification of the method described by Green et al.[45], using a 1.5-fold excess of Zn dust in THF.

^1H, ^{19}F and ^{31}P NMR spectra were recorded on Varian Gemini 200 and 300 spectrometers. Chemical shifts are given in ppm and referenced to the residual ^1H solvent shift of a deuterated external sample or H_3PO_4 (85%, ^{31}P) or trifluorotoluene (^{19}F). The assignment of ^1H and ^{13}C NMR resonances was based on selective ^1H NMR homo decoupling and DEPT experiments. UV/Vis spectra were recorded on a Cary 1E UV/Visible spectrometer. Luminescence spectra were recorded on a Perkin-Elmer Luminescence LS 50B spectrometer. Mass spectra were measured with a Finnigan/MAT 8320 (MS) spectrometer and the peak assignments confirmed by a simulation of the isotope patterns. Magnetic susceptibility measurements were carried out with a Johnson-Matthey laboratory magnetic balance and are reported for 298 K. The susceptibilities were corrected for diamagnetic contributions of the ligands. CHN-analyses were carried out with a LECO CHNS-932 elemental analyzer in our institute. The stochiometric incorporation of solvent molecules into some of the analytically pure compounds was confirmed by either X-ray analysis or ^1H NMR integration.

Electrochemical measurements: Electrochemical measurements were carried out with a BAS 100 B Electrochemical Analyzer. For the electrochemical experiments acetonitrile (Chromasolv, Fluka) was purified as described in the literature,[58] THF (Chromasolv, Fluka) was purified on alumina (Woelm, acidic, super I) and distilled from sodium/benzophenone. Water was purified using a Millipore Milli-Q water purification system. NBu_4PF_6 was used as supporting electrolyte in acetonitrile and THF and was crystallized twice from methanol and dried at 100 °C at 10^{-5} Torr prior to use. NBu_4Br (Fluka) was used as supporting electrolyte in water without further purification. The reversibility of the one-electron transfer processes in the cyclic voltammetry experiments was proven by the criteria $\Delta E_p =$

56 mV, $I_{pa} = I_{pc}$ and the linear behavior of ln(I_{pc}) vs ln (scan speed) (slope 0.5).

Synthesis of [Cp*W(bpy)Cl$_3$], 1-H: A solution of [Cp*W(bpy)Cl$_2$], **2**-H, (499 mg, 0.914 mmol) and C_2Cl_6 (108 mg, 0.456 mmol) in CH_2Cl_2 (15 mL) was stirred for 12 h at RT. A violet precipitate formed and was collected by centrifugation, washed with CH_2Cl_2 and finally dried in high vacuo (458 mg, 86 %); MS (EI): *m*/*z*: 582 [M^+]; $\mu_{eff} = 0.33\ \mu_B$; elemental analysis calcd for $C_{20}H_{23}N_2Cl_3W$: C 41.30, H 3.99, N 4.82, found: C 41.18, H 3.59, N 4.78.

Synthesis of [Cp*W(Cl$_2$bpy)Cl$_2$], 2-Cl: A suspension of [Cp*WCl$_2$]$_2$ (606 mg, 0.777 mmol) and Cl$_2$bpy (351 mg, 1.560 mmol) was degassed in a Schlenk tube equipped with a Young's high-vacuum tap by three freeze-pump-thaw cycles and then stirred at 120 °C. After 24 h the reaction mixture was allowed to cool to RT, filtered and the solvent evaporated in vacuo. The black residue obtained was first washed with toluene until the washings remained colorless and then redissolved in THF. The insoluble solid was crystallized from a mixture of pentanes and THF at −36 °C. Black crystals were obtained, which were separated from the solution by filtration, washed with pentanes and dried under high vacuum (320 mg, 33 %); ^{1}H NMR (CD_2Cl_2): $\delta = 22.8$ (br, $\omega_{1/2} = 85$ Hz), 12.2 (br, $\omega_{1/2} = 140$ Hz), 8.8 (br, $\omega_{1/2} = 40$ Hz), −7 (br, $\omega_{1/2} = 530$ Hz); MS (EI): *m*/*z*: 615 [M^+]; $\mu_{eff} = 1.74\ \mu_B$; elemental analysis calcd for $C_{20}H_{21}Cl_4N_2W$: C 39.06, H 3.44, N 4.55; found: C 39.1, H 3.53, N 4.59.

Synthesis of [Cp*W(Cl$_2$bpy)Cl$_3$], 1-Cl: A solution of [Cp*W(Cl$_2$bpy)Cl$_2$] (214 mg, 0.348 mmol) and hexachloroethane (42 mg, 0.177 mmol) in CH_2Cl_2 (20 mL) was stirred for 4 d at RT. After that time the solvent was evaporated in vacuo and the remaining blue solid was washed with THF and pentanes and finally dried under high vacuum (170 mg, 75 %). ^{1}H NMR (CD_2Cl_2): $\delta = 8.9$ (br, $\omega_{1/2} = 20$ Hz, 2H; Cl$_2$*bpy*), 8.24 (br, $\omega_{1/2} = 15$ Hz, 2H; Cl$_2$*bpy*), 7.7 (br, $\omega_{1/2} = 30$ Hz, 2H; Cl$_2$*bpy*), 1.73 (br, $\omega_{1/2} = 20$ Hz, 15H; C_5Me_5); $\mu_{eff} = 0.78\ \mu_B$; elemental analysis calcd for $C_{20}H_{21}Cl_5N_2W$: C 36.93, H 3.25, N 4.31; found: C 37.25, H 3.34, N 4.50.

[(Cp*W((NMe$_2$)$_2$bpy)(μ-O))$_2$][PF$_6$]$_2$, 3-NMe$_2$: Complex [(Cp*W((NMe$_2$)$_2$bpy)(μ-O))$_2$][PF$_6$]$_2$ was synthesized by hydrolysis of [Cp*W((NMe$_2$)$_2$bpy)Cl$_3$] (325 mg, 0.527 mmol) in degassed water (15 mL) following the same procedure as for complex [(Cp*W(bpy)-(μ-O))$_2$][PF$_6$]$_2$. Due to its low solubility in methylenechloride, acetonitrile was used for the extraction step. After crystallization from Et$_2$O/acetonitrile (1:1) the analytically pure material was obtained as green crystals (308 mg, 81 %). ^{1}H NMR (CD_3CN): $\delta = 7.73$ (d, $^3J = 7$ Hz, 4H; (NMe$_2$)$_2$*bpy*), 6.82 (d, $^4J = 3$ Hz, 4H; (NMe$_2$)$_2$*bpy*), 6.33 (dd, $^3J = 7$, $^4J = 3$ Hz, 4H; (NMe$_2$)$_2$*bpy*), 3.10 (s, 24H; (N*Me*$_2$)$_2$bpy), 1.66 (br s, $\omega_{1/2} \approx 8$ Hz, 30H; C_5Me_3); ^{19}F NMR (CD_3CN): $\delta = -73.1$ (d, $^1J_{PF} = 712$ Hz); UV/Vis (CH_2Cl_2): λ_{max} (ε) = 599 nm (7×10^3 L mol^{-1} cm^{-1}); MS (FAB$^+$, CH_3CN): *m*/*z*: 577 [M^{2+}]; elemental analysis calcd for $C_{48}H_{66}F_{12}N_8O_2P_2W_2$: C 39.91, H 4.60, N 7.76, found: C 40.12, H 4.29, N 7.71.

[(Cp*W((NMe$_2$)$_2$bpy)(μ-O))$_2$][BPh$_4$]$_2$, 3^{BPh_4}-NMe$_2$: A mixture of [(Cp*W((NMe$_2$)$_2$bpy)(μ-O))$_2$][PF$_6$]$_2$ (51 mg, 0.071 mmol) and NaBPh$_4$ (4 mg, 0.071 mmol) was stirred in THF (10 mL). After 30 min the solvent was removed in vacuo and the residue was extracted with CH_2Cl_2. After filtration over a pad of Celite and addition of small amounts of Et$_2$O the product crystallized as green needles from the deep green solution at −36 °C, which were separated from the solution, washed with Et$_2$O and dried under high vacuum (56 mg, 90 %). Suitable single crystals for X-ray diffraction were obtained by crystallization from Et$_2$O/acetone (1:1) at room temperature. ^{1}H NMR (CD_3CN): $\delta = 7.72$ (d, $^3J = 7$ Hz, 4H; (NMe$_2$)$_2$*bpy*), 7.26 (m, 16H; [B*Ph*$_4$]$^-$), 6.98 (m, 16H; [B*Ph*$_4$]$^-$), 6.83 (m, 12H; [B*Ph*$_4$]$^-$, (NMe$_2$)$_2$*bpy*), 6.31 (dd, $^3J = 7$, $^4J = 3$ Hz, 4H; (NMe$_2$)$_2$*bpy*), 3.08 (s, 24H; (N*Me*$_2$)$_2$bpy), 1.54 (s, 30H; C_5Me_3); MS (FAB$^+$, CH_2Cl_2): *m*/*z*: 577 [M^{2+}]; elemental analyis calcd for $C_{96}H_{106}B_2N_8O_2W_2$: C 64.30, H 5.96, N 6.25; found: C 64.47, H 5.91, N 6.22.

[(Cp*W(*t*Bu$_2$bpy)(μ-O))$_2$][PF$_6$]$_2$, 3-*t*Bu: Complex [(Cp*W(*t*Bu$_2$bpy)-(μ-O))$_2$][PF$_6$]$_2$ was synthesized by hydrolysis of [Cp*W(*t*Bu$_2$bpy)Cl$_3$] (1.04 g, 1.50 mmol) in degassed water (50 mL) following the same procedure as described for complex [(Cp*W(bpy)(μ-O))$_2$][PF$_6$]$_2$ to yield black crystals (918 mg, 82 %). ^{1}H NMR (CD_3CN): $\delta = 8.40$ (d, $^3J = 6$ Hz, 4H; *t*Bu$_2$*bpy*), 7.91 (d, $^4J = 2$ Hz, 4H; *t*Bu$_2$*bpy*), 7.32 (dd, $^3J = 6$, $^4J = 2$ Hz, 4H; *t*Bu$_2$*bpy*), 1.48 (s, 30H; C_5Me_5), 1.28 (s, 18H; *tBu*$_2$bpy); ^{13}C{^{1}H} NMR ([D$_6$]acetone): $\delta = 166.4$ (s, quart. C; *t*Bu$_2$*bpy*), 153.6 (s, CH; *t*Bu$_2$*bpy*), 151.9 (s, quart. C; *t*Bu$_2$*bpy*), 123.0 (s, CH; *t*Bu$_2$*bpy*), 120.8 (s, CH; *t*Bu$_2$*bpy*), 113.9 (s, quart. C; C_5Me_5), 36.2 (s, quart. C; *tBu*$_2$bpy), 30.6 (s, CH_3; *tBu*$_2$bpy), 9.5 (s, CH_3; C_5Me_5); ^{31}P NMR ([D$_6$]acetone): $\delta = -145.0$ (sept, $^1J_{FP} = 714$ Hz); MS (FAB$^+$): *m*/*z*: 603 [M^{2+}]; UV/Vis (CH_2Cl_2): λ (ε) = 775 (0.6×10^4), 608 (1.6×10^4), 480 nm (0.7×10^4 mol L^{-1} cm^{-1}); elemental analysis calcd for $C_{56}H_{78}F_{12}N_4O_2P_2W_2$: C 44.93, H 5.25, N 3.74; found: C 45.19, H 5.38, N 3.77.

[(Cp*W(*t*Bu$_2$bpy)(μ-O))$_2$][BPh$_4$]$_2$, 3^{BPh_4}-*t*Bu: A mixture of [(Cp*W(*t*Bu$_2$bpy)(μ-O))$_2$][PF$_6$]$_2$ (166 mg, 0.110 mmol) and NaBPh$_4$ (90 mg, 0.260 mmol) was stirred in THF (10 mL) at RT. After 30 min the solvent was removed in vacuo and the residue was extracted into CH_2Cl_2. After filtration over a pad of Celite and addition of a small amount of Et$_2$O, the product crystallized from the deep blue solution at room temperature as black crystals, which were separated from the solution, washed with Et$_2$O and dried under high vacuo (192 mg, 95 %). Suitable single crystals for X-ray diffraction were obtained by crystallization from Et$_2$O/CH_2Cl_2 at RT. ^{1}H NMR (CD_3CN): $\delta = 8.38$ (d, $^3J = 6$ Hz, 4H; *t*Bu$_2$*bpy*), 7.92 (d, $^4J = 2$ Hz, 4H; *t*Bu$_2$*bpy*), 7.31 (dd, $^3J = 6$, $^4J = 2$ Hz, 4H; *t*Bu$_2$*bpy*), 7.26 (m, 16H; [B*Ph*$_4$]$^-$), 7.00 (m, 16H; [B*Ph*$_4$]$^-$), 6.83 (m, 8H; [B*Ph*$_4$]$^-$), 1.47 (s, 30H; C_5Me_5), 1.28 (s, 18H; *tBu*$_2$bpy); ^{13}C{^{1}H} NMR (CD_3CN): $\delta = 166.5$ (s, quart. C; *t*Bu$_2$*bpy*), 153.6 (s, CH; *t*Bu$_2$*bpy*), 152.1 (s, quart. C; *t*Bu$_2$*bpy*), 137.1 (q, $J_{B,C} = 3$ Hz, CH; [B(C_6H_6)$_4$]$^-$), 126.9 (q, $J_{B,C} = 6$ Hz, CH; [B(C_6H_6)$_4$]$^-$), 123.1, 123.0 (2 s, CH, *t*Bu$_2$*bpy*; [B(C_6H_6)$_4$]$^-$), 121.6 (s, CH; *t*Bu$_2$*bpy*), 114.3 (s, quart. C; C_5Me_5), 36.6 (s, quart. C; *tBu*$_2$bpy), 31.1 (s, CH_3; *tBu*$_2$bpy), 9.9 (s, CH_3; C_5Me_5); elemental analysis calcd for $C_{104}H_{118}B_2N_4O_2W_2$: C 67.69, H 6.44, N 3.04, found: C 67.61, H 6.20, N 3.08.

[Cp*W(Me$_2$bpy)(μ-O))$_2$][PF$_6$]$_2$, 3-Me: Complex [(Cp*W(Me$_2$bpy)-(μ-O))$_2$][PF$_6$]$_2$ was synthesized by hydrolysis of [Cp*W(Me$_2$bpy)Cl$_3$] (336 mg, 0.551 mmol) in degassed water (15 mL) following the same procedure as described for complex [(Cp*W(bpy)(μ-O))$_2$][PF$_6$]$_2$. Suitable single crystals for X-ray diffraction were obtained by crystallization from Et$_2$O/acetone at RT as black crystals (346 mg, 95 %). ^{1}H NMR (CD_3CN): $\delta = 8.14$ (d, $^3J = 6$ Hz, 4H; Me$_2$*bpy*), 7.70 (s, 4H; Me$_2$*bpy*), 7.07 (d, $^3J = 6$ Hz, 4H; Me$_2$*bpy*), 2.52 (s, 12H; *Me*$_2$bpy), 1.53 (s, 30H; C_5Me_5); ^{13}C{^{1}H} NMR (CD_2Cl_2): $\delta = 154.0$ (s, quart. C; Me$_2$*bpy*), 152.9 (s, CH; Me$_2$*bpy*), 151.4 (s, quart. C; Me$_2$*bpy*), 127.3 (s, CH; Me$_2$*bpy*), 123.4 (s, CH; Me$_2$*bpy*), 114.0 (s, quart. C; C_5Me_5), 21.3 (s, CH_3; *Me*$_2$bpy), 10.2 (s; $C_5(CH_3)_5$); ^{31}P NMR (CD_2Cl_2): $\delta = -145.2$ (sept., $^1J_{FP} = 715$ Hz); ^{19}F NMR (CD_2Cl_2): $\delta = -73.93$ (d, $^1J_{PF} = 715$ Hz); MS (FAB$^+$): *m*/*z*: 519 [M^{2+}]; UV/Vis (CH_2Cl_2): λ (ε) = 773 (3×10^3), 608 (5×10^3 mol L^{-1} cm^{-1}), 500 nm (not determ.); elemental analysis calcd for $C_{44}H_{54}F_{12}N_4O_2P_2W_2$: C 39.78, H 4.10, N 4.22, found: C 39.41, H 3.92, N 4.09.

[(Cp*W(Me$_2$bpy)(μ-O))$_2$][Cl]$_2$, 3^{Cl}-Me: A mixture of [Cp*W(Me$_2$bpy)Cl$_3$] (134 mg, 0.220 mmol) and $NaHCO_3$ (37 mg, 0.440 mmol) was stirred for 1 h in degassed water (5 mL) at 80 °C. After evaporation of the solvent in vacuo, the residue was extracted with CH_2Cl_2. The solvent was removed in vacuo and the dark violet product was dried at 70 °C under high vacuum to remove residual CH_2Cl_2 (118 mg, 96 %). H NMR (CD_3CN): $\delta = 8.14$ (d, $^3J = 6$ Hz, 4H; Me$_2$*bpy*), 8.09 (d, $^4J = 2$ Hz, 4H; Me$_2$*bpy*), 7.11 (dd, $^3J = 6$ Hz, $^4J = 2$ Hz, 4H; Me$_2$*bpy*), 2.55 (s, 12H; *Me*$_2$bpy), 1.52 (s, 30H; C_5Me_5); ^{1}H NMR (D_2O): $\delta = 8.02$ (d, $^3J = 6$ Hz, 4H; Me$_2$*bpy*), 7.67 (s, 4H; Me$_2$*bpy*), 7.02 (d, $^3J = 6$ Hz, 4H; Me$_2$*bpy*), 2.39 (s, 12H; *Me*$_2$bpy), 1.41 (s, 30H; C_5Me_5); ^{13}C{^{1}H} NMR (CD_3CN): $\delta = 153.9$ (s, quart. C; Me$_2$*bpy*), 153.3 (s, CH; Me$_2$*bpy*), 151.6 (s, quart. C; Me$_2$*bpy*), 127.5 (s, CH; Me$_2$*bpy*), 124.3 (s, CH; Me$_2$*bpy*), 113.8 (s, quart. C; C_5Me_5), 21.0 (s, CH_3; *Me*$_2$bpy), 9.7 (s; $C_5(CH_3)_5$); elemental analysis calcd for $C_{44}H_{54}Cl_2N_4O_2W_2$: C 47.63, H 4.91, N 5.05, found: C 47.76, H 4.69, N 5.04.

Synthesis of [(Cp*W(bpy)(μ-O))$_2$][PF$_6$]$_2$, 3-H: The stirring of the reaction mixture of [Cp*W(bpy)Cl$_3$] (449 mg, 0.771 mmol) in water (10 mL) gave a homogeneous dark gave a red solution (pH 1). After neutralization by the addition of solid $NaHCO_3$, a solution of NH_4PF_6 (127 mg, 0.779 mmol) in water (5 mL) was added slowly and a dark blue solid precipitated. The solvent was removed under reduced pressure and the remaining solid was extracted with CH_2Cl_2. After filtration over a pad of Celite the product was precipitated through the addition of Et$_2$O. The analytically pure solid was collected by filtration and dried in high vacuum to yield black crystals (413 mg, 84 %). ^{1}H NMR ([D$_6$]acetone): $\delta = 8.69$ (d, $^3J = 5.0$ Hz, 4H; *bpy*), 8.21 (d, $^3J = 8.2$ Hz, 4H; *bpy*), 7.86 (dt, $^3J = 8.2$ Hz, $^3J = 7.1$ Hz, 4H; *bpy*), 7.52 (dt, $^3J = 5.0$ Hz, $^3J = 7.1$ Hz, 4H; *bpy*), 1.64 (s, 30H; $C_5(CH_3)_5$); ^{13}C{^{1}H} NMR ([D$_6$]acetone): $\delta = 154.0$ (s, CH; *bpy*), 151.6 (s, quart. C; *bpy*), 141.3 (s, CH; *bpy*), 127.0 (s, CH; *bpy*), 123.6 (s, CH; *bpy*), 114.6 (s, quart. C; C_5Me_5), 9.61 (s; $C_5(CH_3)_5$); ^{31}P NMR ([D$_6$]acetone): $\delta = -142.6$ (sept., $^1J_{PF} = 709$ Hz); ^{19}F NMR ([D$_6$]acetone): $\delta = -71.3$ (d, $^1J_{FP} = 709$ Hz); MS (FAB$^+$): *m*/*z*: 491 [M^{2+}]; UV/Vis (CH_2Cl_2): λ = 790, 612 nm; elemental

analysis calcd for $C_{40}H_{46}F_{12}N_4O_2P_2W_2$: C 37.76, H 3.64, N 4.40; found: C 37.51, H 3.75, N 4.22.

[(Cp*W(Cl$_2$bpy)(μ-O))$_2$][PF$_6$]$_2$, 3-Cl: Complex [(Cp*W(Cl$_2$bpy)-(μ-O))$_2$][PF$_6$]$_2$ was synthesized by hydrolysis of [Cp*W(Cl$_2$bpy)Cl$_3$] (86 mg, 0.132 mmol) in degassed water (4 mL) following the same procedure as for complex [(Cp*W(bpy)(μ-O))$_2$][PF$_6$]$_2$ to yield green needles (83 mg, 89 %). ^{1}H NMR (CD$_3$CN): $\delta = 8.24$ (d, $^3J = 6$ Hz, 4H; Cl$_2$*bpy*), 8.05 (d, $^4J = 2$ Hz, 4H; Cl$_2$*bpy*), 7.40 (dd, $^3J = 6$, $^4J = 2$ Hz, 4H; Cl$_2$*bpy*), 1.58 (s, 30H; C$_5$*Me*$_5$); ^{13}C{^{1}H} NMR (CD$_3$CN): $\delta = 154.7$ (s, CH; Cl$_2$*bpy*), 151.5 (s, quart. C; Cl$_2$*bpy*), 149.3 (s, quart. C; Cl$_2$*bpy*), 127.5 (s, CH; Cl$_2$*bpy*), 125.1 (s, CH; Cl$_2$*bpy*), 115.8 (s, quart. C; *C*$_5$Me$_5$), 10.2 (s; C$_5$(*C*H$_3$)$_5$); UV/Vis (CH$_2$Cl$_2$): λ_{max} (ε) = 662 nm (5×10^3 L mol^{-1} cm^{-1}); elemental analysis calcd for $C_{40}H_{42}Cl_4F_{12}N_4O_2P_2W_2$: C 34.07, H 3.00, N 3.97; found: C 34.41, H 2.88, N 4.10.

Isolation of [(Cp*W(Me$_2$bpy)(μ-Cl))$_2$(μ-O)][BPh$_4$][Cl], 4-Me: From a solution of [(Cp*W(Me$_2$bpy)Cl$_2$][BPh$_4$][22] in a mixture of Et$_2$O and CH$_2$Cl$_2$, black crystals were separated after several days. Suitable single crystals for X-ray diffraction were obtained by crystallization from Et$_2$O/CH$_2$Cl$_2$ at room temperature. ^{1}H NMR (CD$_2$Cl$_2$): $\delta = 8.61$ (s, 4H$_{3,3'}$), 7.80 (d, $^3J_{HH} = 6$ Hz, 4H$_{6,6'}$), 7.33 (m, 8H; B(*Ph*)$_4^-$), 7.02 (m, 12H, H$_{5,5'}$; B(*Ph*)$_4^-$), 6.86 (m, 4H; B(*Ph*)$_4^-$), 2.54 (s, 12H; *Me*$_2$bpy), 1.88 (s, 30H; (C$_5$*Me*$_5$)); MS (FAB$^+$, CH$_2$Cl$_2$): *m*/*z*: 575 [Cp*W(Me$_2$bpy)Cl$_2$]$^+$; elemental analysis calcd for $C_{68}H_{74}BCl_2N_4OW_2 \cdot CH_2Cl_2$: C 54.06, H 5.00, N 3.65; found: C 54.20, H 4.96, N 3.60.

[(Cp*W(Me$_2$bpy)(μ-O))$_2$][PF$_6$]$_3$, 5-Me: [Cp$_2$Fe][PF$_6$] (38 mg, 0.114 mmol) was added as a solid to a stirred solution of [(Cp*W(Me$_2$bpy)(μ-O))$_2$][PF$_6$]$_2$ (105 mg, 0.079 mmol) in CH$_2$Cl$_2$ (5 mL). After the color of the solution had changed from blue to red, the solvent was removed under reduced pressure. The residue was washed with toluene to remove Cp$_2$Fe until the washings remained colorless and finally dried under high vacuum. The crude product crystallized from Et$_2$O/acetonitrile at −36 °C as red crystals (76 mg, 66 %). Suitable single crystals for X-ray diffraction were obtained by diffusion of Et$_2$O into a solution in acetonitrile at room temperature. ^{1}H NMR (CD$_3$CN): $\delta = \approx 19$ (br, $\omega_{1/2} = 1500$ Hz), 10 (br, $\omega_{1/2} = 100$ Hz), 9 (br, $\omega_{1/2} = 300$ Hz); ^{31}P NMR: $\delta = -145.0$ (sept., $^1J_{P,F} = 714$ Hz, $\omega_{1/2} = 10$ Hz); ^{19}F NMR (CD$_3$CN): $\delta = -72.3$ (d, $^1J_{F,P} = 714$ Hz, $\omega_{1/2} = 10$ Hz); MS (FAB$^+$, CH$_3$CN): *m*/*z*: 519 [M^{2+}]; $\mu_{eff} = 1.55$ μ_B; elemental analysis calcd for $C_{44}H_{54}F_{18}N_4O_2P_3W_2$: C 35.87, H 3.69, N 3.80; found: C 36.18, H 3.23, N 4.27.

[(Cp*W(*t*Bu$_2$bpy)(μ-O))$_2$], 6-*t*Bu: A solution of sodium naphthalenide freshly prepared by stirring naphthalene (18 mg, 0.140 mmol) with an excess of sodium in THF (5 mL), was dropped into a suspension of [(Cp*W(*t*Bu$_2$bpy)(μ-O))$_2$][PF$_6$]$_2$ (105 mg, 0.070 mmol) in THF (5 mL) under vigorous stirring. The solvent was removed from the resulting violet solution under reduced pressure and the residue was treated three times with pentanes to remove residual THF. The solid residue was extracted with pentanes (30 mL) and the violet pentane solution was filtered over a glass fiber filter and dried in vacuo. The crude product was redissolved several times in pentanes and dried under high vacuum to remove residual naphthalene to yield a dark violet powder (66 mg, 79 %). ^{1}H NMR ([D$_6$]benzene): $\delta = 9.93$ (d, $^3J = 8$ Hz, 4H; *t*Bu$_2$*bpy*), 7.82 (d, $^4J = 2$ Hz, 4H; *t*Bu$_2$*bpy*), 6.06 (dd, $^3J = 8$ Hz, $^4J = 2$ Hz, 4H; *t*Bu$_2$*bpy*), 1.34 (s, 36H; *t*Bu$_2$bpy), 1.02 (s, 30H; C$_5$*Me*$_5$); ^{13}C{^{1}H} NMR ([D$_6$]benzene): $\delta = 144.7$ (s, CH; *t*Bu$_2$*bpy*), 140.5 (s, quart. C; *t*Bu$_2$*bpy*), 134.4 (s, quart. C; *t*Bu$_2$*bpy*), 113.7 (s, CH; *t*Bu$_2$*bpy*), 109.4 (s, CH; *t*Bu$_2$*bpy*), 108.4 (s, quart. C; *C*$_5$Me$_5$), 33.1 (s, quart. C; *t*Bu$_2$bpy), 30.9 (s, CH$_3$; *t*Bu$_2$bpy), 8.4 (s, CH$_3$; C$_5$*Me*$_5$); MS (EI): *m*/*z*: 1206 [M^+]; elemental analysis calcd for $C_{56}H_{78}N_4O_2W_2$: C 55.73, H 6.51, N 4.64; found: C 56.00, H 6.73, N 4.58.

[(Cp*W(Me$_2$bpy)(μ-O))$_2$], 6-Me, and [(Cp*W(Me$_2$bpy)(μ-O))$_2$][PF$_6$], 7-Me: A solution of sodium naphthalenide freshly prepared by stirring naphthalene (21 mg, 0.160 mmol) with an excess of sodium in THF (5 mL), was dropped into a suspension of [(Cp*W(Me$_2$bpy)(μ-O))$_2$][PF$_6$]$_2$ (109 mg, 0.082 mmol) in THF (5 mL) under vigorous stirring. The solvent was removed from the resulting violet solution under reduced pressure and the residue washed three times with pentanes and extracted with toluene. First a violet fraction was collected, followed by a second brown fraction. The violet toluene fraction was filtered over a glass fiber filter and the solvent was removed in vacuo. To remove residual naphthalene the crude product was redissolved several times in toluene and dried under high vacuum to yield the analytically pure complex [(Cp*W(Me$_2$bpy)(μ-O))$_2$] (25 mg, 29 %). From the brown toluene fraction the solvent was removed in vacuo and the obtained green solid was crystallized from Et$_2$O/THF to yield complex [(Cp*W(Me$_2$bpy)(μ-O))$_2$][PF$_6$] (26 mg, 27 %). For complex [(Cp*W(Me$_2$bpy)(μ-O))$_2$], suitable single crystals for X-ray diffraction were obtained from a toluene solution after several days at room temperature. For complex [(Cp*W(Me$_2$bpy)(μ-O))$_2$][PF$_6$], single crystals were obtained by crystallization from Et$_2$O/THF at room temperature. Analytical data for complex [(Cp*W(Me$_2$bpy)(μ-O))$_2$]: ^{1}H NMR ([D$_8$]THF): $\delta = 9.60$ (d, $^3J = 8$ Hz, 4H; Me$_2$*bpy*), 7.40 (d, $^4J = 2$ Hz, 4H; Me$_2$*bpy*), 5.70 (dd, $^3J = 8$ Hz, $^4J = 2$ Hz, 4H; Me$_2$*bpy*), 2.60 (s, 12H; *Me*$_2$bpy), 0.85 (s, 30H; C$_5$*Me*$_5$); elemental analysis calcd for $C_{44}H_{54}N_4O_2W_2 \cdot C_7H_8$: C 54.17, H 5.53, N 4.95; found: C 54.02, H 5.60, N 5.03. Analytical data for complex [(Cp*W(Me$_2$bpy)(μ-O))$_2$][PF$_6$]: ^{1}H NMR ([D$_8$]THF): $\delta =$ 10 (br, $\omega_{1/2} = 300$ Hz), −6 (v br). No satisfying elemental analysis could be obtained for this compound.

Reaction of [(Cp*W(*t*Bu$_2$bpy)(μ-O))$_2$], 6-*t*Bu, with HOTf in [D$_8$]THF: When a solution of (Cp*W(*t*Bu$_2$bpy)(μ-O))$_2$ (35 mg, 0.029 mmol) in [D$_8$]THF was mixed with approximately 4 equiv HOTf in a Teflon sealed NMR tube, the color of the solution changed immediately from violet to red and a black precipitate formed. The ^{1}H NMR spectrum showed a singlet at $\delta = 4.55$. The solvent was vacuum transferred into another NMR tube and a ^{1}H NMR spectrum of the volatiles also showed a singlet at $\delta =$ 4.55. The non-volatile residue was washed with Et$_2$O and toluene and dissolved in methylenechloride. Residual HOTf was neutralized by addition of a small amount of NaHCO$_3$, which was indicated by a color change from red to blue. The solution was filtered and the solvent was removed under reduced pressure to yield a black powder (26 mg, 60 % based on [(Cp*W(*t*Bu$_2$bpy)(μ-O))$_2$]. The ^{1}H NMR resonances (CD$_3$CN) of the product were identical to those of complex [(Cp*W(*t*Bu$_2$bpy)(μ-O))$_2$][PF$_6$]$_2$.

[(Cp*W(Me$_2$bpy)(μ-O)(μ-OH)][PF$_6$]$_2$[OTf], 8-Me: Trifluoromethanesulfonic acid (5.65 μL, 0.065 mmol) was added to a stirred solution of [(Cp*W(Me$_2$bpy)(μ-O))$_2$][PF$_6$]$_2$ (86 mg, 0.065 mmol) in methylenechloride (10 mL), which led to an immediate color change from blue to red. The solution was filtered and the solvent reduced to 5 mL by evaporation. By slow addition of Et$_2$O, red crystals were obtained, which were collected, washed with Et$_2$O and dried in vacuo (62 mg, 65 %). ^{1}H NMR (CD$_2$Cl$_2$): $\delta = 12.3$ (br s, 1H), 8.40 (d, $^3J = 6$ Hz, 2H; Me$_2$*bpy*), 8.16 (s, 4H; Me$_2$*bpy*), 8.11 (d, $^3J = 6$ Hz, 2H; Me$_2$*bpy*), 7.42 (d, $^3J = 6$ Hz, 2H; Me$_2$*bpy*), 7.31 (d, $^3J = 6$ Hz, 2H; Me$_2$*bpy*), 2.63 (s, 6H; *Me*$_2$bpy), 2.62 (s, 6H; *Me*$_2$bpy), 1.79 (s, 30H; C$_5$*Me*$_5$); ^{13}C{^{1}H} NMR (CD$_2$Cl$_2$): $\delta = 156.5$ (s, quart. C; Me$_2$*bpy*), 156.4 (s, quart. C; Me$_2$*bpy*), 155.7 (s, CH; Me$_2$*bpy*), 152.8 (s, CH; Me$_2$*bpy*), 152.5 (s, quart. C; Me$_2$*bpy*), 152.0 (s, quart. C; Me$_2$*bpy*), 130.2 (s, CH; Me$_2$*bpy*), 129.1 (s, CH; Me$_2$*bpy*), 125.9 (s, CH; Me$_2$*bpy*), 125.5 (s, CH; Me$_2$*bpy*), 118.0 (s, quart. C; *C*$_5$Me$_5$), 21.3 (s; *Me*$_2$bpy), 21.2 (s; *Me*$_2$bpy), 10.0 (s; C$_5$*Me*$_5$); ^{19}F NMR (CD$_2$Cl$_2$): $\delta = 73.75$ (d, $^1J_{PF} = 720$ Hz; P*F*$_6^-$), −80.30 (s; (*C*F$_3$)SO$_3^-$); ^{31}P NMR (CD$_2$Cl$_2$): $\delta = -145.19$ (m, $^1J_{FP} = 720$ Hz); elemental analysis calcd for $C_{45}H_{55}F_{15}N_4O_5P_2SW_2$: C 36.55, H 3.75, N 3.79; found: C 36.76, H 3.95, N 3.63.

X-ray crystal structure analyses

General remarks: Suitable single crystals were mounted on glass fibers in polyisobutylene oil (Aldrich 38 896-6), transferred on the goniometer head to the diffractometer and the crystal was cooled to −90 °C in a N$_2$ cryostream. The data sets were collected with graphite monochromated Mo$_{K\alpha}$ radiation (0.70713 Å) on a Siemens-P3 four-circle diffractometer (**3**-Me) and a Stoe IPDS image plate diffractometer (all others). Intensities were corrected for Lorentz and polarization effects. Absorption corrections were performed using Ψ scans (**3**-Me) or numerically (all others). The structures were solved using direct methods with the SHELXS-97 program.[59] The refinements were carried out with SHELXL-97 using all unique F_o^2.[60] Except for **3**-Me and **5**-Me all non-hydrogen atoms were treated anisotropically with the positions of the hydrogen atoms calculated in idealized positions (C−H bonds fixed at 0.96 Å) and refined as riding model. The details of the data collections and refinements including *R* values are summarized in Tables 4 and 9.

Crystallographic data have been deposited with the Cambridge Crystallographic Data center as supplementary publication numbers CCDC-191 011 (**3**-Me), -191 012 (**3**^{BPh_4}-*t*Bu), -191 013 (**3**^{BPh_4}-NMe$_2$), -191 014 (**5**-Me), -191 015 (**6**-Me), and -191 016 (**7**-Me). Copies of the data can be obtained free of charge on application to CCDC, 12 Union Road, Cambridge CB2 1EZ, UK [Fax: (+44) 1223 336-033; E-mail: deposit@ccdc.cam.ac.uk].

Table 9. Data collection parameters of complexes **5**-Me, **6**-Me and **7**-Me.

	5-Me	**6**-Me	**7**-Me
formula	$C_{44}H_{54}F_{18}N_4O_2P_3W_2 \cdot 2\,MeCN$	$C_{44}H_{54}N_4O_2W_2 \cdot 2$ toluene	$C_{44}H_{54}F_6N_4O_2PW_2$
F_w	1549.60	1222.8	1183.56
habitus	orange rect. parallelepiped	violet cube	green rect. parallelepiped
crystal dimension [mm]	$0.2 \times 0.2 \times 0.1$	$0.2 \times 0.2 \times 0.2$	$0.3 \times 0.3 \times 0.2$
crystal system	monoclinic	monoclinic	monoclinic
space group	$P2_1/n$ (No 14)	$P2_1/c$ (No 14)	$I2/a$ (No 15)
a [Å]	11.675(1)	15.399(1)	22.609(1)
b [Å]	36.925(1)	10.415(1)	25.569(1)
c [Å]	13.207(1)	16.649(1)	29.682(2)
α [°]			
β [°]	102.36(1)	109.51(1)	95.70(3)
V [Å^3]	5561.6(7)	2516.9(3)	17074.0(15)
Z	4	4	8
ρ_{calcd} [g cm^{-3}]	1.85	1.61	1.83
μ [mm^{-1}]	4.32	4.61	5.48
$F(000)$	3020	1188	9192
T [K]	183(2)	183(2)	183(2)
2θ [°]	4–44	4–52	2–48
no. measured reflections (total unique)	12000, 6635	9515, 4515	13179, 13179
no. of parameters	684	326	1100
R_1 ($F^2 < 2\sigma F^2$)	0.0575	0.0252	0.0279
wR_2 ($F^2 < 2\sigma F^2$)	0.1582	0.0612	0.0683
GoF, S	1.15	1.00	0.97
res. el. dens. [e$^-$ Å^{-3}]	2.40, −1.26	2.41, −1.37	1.61, −1.89

Acknowledgement

We are indebted to Prof. Heinz Berke for his generous support. Funding of this project by the Swiss National Science Foundation is gratefully acknowledged.

[1] R. Poli, *Chem. Rev.* **1991**, *91*, 509.
[2] E. Le Grognec, R. Claverie, R. Poli, *J. Am. Chem. Soc.* **2001**, *123*, 9513.
[3] E. Le Grognec, R. Poli, *Chem. Eur. J.* **2001**, *7*, 4572.
[4] J. M. Camus, D. Morales, J. Andrieu, P. Richard, R. Poli, P. Braunstein, F. Naud, *J. Chem. Soc. Dalton Trans.* **2000**, 2577.
[5] R. Poli, *Synlett* **1999**, 1019.
[6] R. Poli, *Chem. Rev.* **1996**, *96*, 2135.
[7] T. E. Glassman, M. G. Vale, R. R. Schrock, *Organometallics* **1991**, *10*, 4046.
[8] R. R. Schrock, A. H. Liu, M. B. O'Regan, W. C. Finch, J. F. Payack, *Inorg. Chem.* **1988**, *27*, 3574.
[9] M. B. O'Regan, A. H. Liu, W. C. Finch, R. R. Schrock, M. D. Davis, *J. Am. Chem. Soc.* **1990**, *112*, 4331.
[10] R. C. Murray, L. Blum, A. H. Liu, R. R. Schrock, *Organometallics* **1985**, *4*, 953.
[11] X. Morise, M. L. H. Green, P. C. McGowan, S. J. Simpson, *J. Chem. Soc. Dalton Trans.* **1994**, 871.
[12] M. L. H. Green, P. C. Konidaris, P. Mountford, *J. Chem. Soc. Dalton Trans.* **1994**, 2851.
[13] M. L. H. Green, P. C. McGowan, X. Morise, *Polyhedron* **1994**, *13*, 2971.
[14] A. H. Liu, R. C. Murray, J. C. Dewan, B. D. Santarsiero, R. R. Schrock, *J. Am. Chem. Soc.* **1987**, *109*, 4282.
[15] R. R. Schrock, T. E. Glassman, M. G. Vale, M. Kol, *J. Am. Chem. Soc.* **1993**, *115*, 1760.
[16] H. Blackburn, J. C. Fettinger, H. B. Kraatz, R. Poli, R. C. Torralba, *J. Organomet. Chem.* **2000**, *594*, 27.
[17] B. Pleune, R. Poli, J. C. Fettinger, *Organometallics* **1997**, *16*, 1581.
[18] H. Blackburn, H. B. Kraatz, R. Poli, R. C. Torralba, *Polyhedron* **1995**, *14*, 2225.
[19] R. T. Baker, J. C. Calabrese, R. L. Harlow, I. D. Williams, *Organometallics* **1993**, *12*, 830.
[20] Q. Feng, M. Ferrer, M. L. H. Green, P. Mountford, V. S. B. Mtetwa, *J. Chem. Soc. Dalton Trans.* **1992**, 1205.
[21] S. J. Holmes, R. R. Schrock, *Organometallics* **1983**, *2*, 1463.
[22] C. Cremer, P. Burger, *J. Chem. Soc. Dalton Trans.* **1999**, 1967.
[23] C. Cremer, P. Burger, *J. Am. Chem. Soc.* **2003**, *125*, ASAP (DOI: 10.1021/ja028313e).
[24] G. B. Deacon, T. Feng, S. Nickel, B. W. Skelton, A. H. White, *Chem. Commun.* **1993**, 1328.
[25] C. Hansch, A. Leo, R. W. Taft, *Chem. Rev.* **1991**, *91*, 165.
[26] N. G. Connelly, P. R. G. Davis, E. E. Harry, P. Klangsinsirikul, M. Venter, *J. Chem. Soc. Dalton Trans.* **2000**, 2273.
[27] K. M. Kadish, *Prog. Inorg. Chem.* **1986**, *34*, 435.
[28] T. Ren, C. Lin, E. J. Valente, J. D. Zubkovski, *Inorg. Chim. Acta* **2000**, *297*, 283.
[29] T. Ren, *Coord. Chem. Rev.* **1998**, *175*, 43.
[30] A. Giraudeau, H. J. Callot, J. Jordan, I. Ezhar, M. Gross, *J. Am. Chem. Soc.* **1979**, *101*, 3857.
[31] C. Creutz, *Prog. Inorg. Chem.* **1983**, *30*, 1.
[32] M. B. Robin, P. Day, *Adv. Inorg. Chem. Radiochem.* **1967**, *10*, 247.
[33] C. Cremer, P. Burger, unpublished results.
[34] R. Poli, *Chem. Rev.* **1991**, *91*, 509.
[35] B. E. Bursten, R. H. Cayton, *Inorg. Chem.* **1989**, *28*, 2846.
[36] W. A. Herrmann, R. A. Fischer, J. K. Felixberger, R. A. Paciello, P. Kiprof, E. Herdtweck, *Z. Naturforsch.* **1988**, *43b*, 1391.
[37] M. Cousins, M. L. H. Green, *J. Chem. Soc.* **1964**, 1567.
[38] C. Couldwell, K. Prout, *Acta Crystallogr. Sect. B* **1978**, *34*, 933.
[39] F. Abugideiri, G. A. Brewer, J. U. Desai, J. C. Gordon, R. Poli, *Inorg. Chem.* **1994**, *33*, 3745.
[40] A. G. Orpen, L. Brammer, F. H. Allen, O. Kennard, D. G. Watson, R. Taylor, *J. Chem. Soc. Dalton Trans.* **1989**, S1.
[41] J. C. Green, M. L. H. Green, P. Mountford, J. Parkington, *J. Chem. Soc. Dalton Trans.* **1990**, 3407.
[42] F. Abugideiri, J. C. Fettinger, R. Poli, *Inorg. Chim. Acta* **1995**, *229*, 445.
[43] P. Schollhammer, F. Y. Pétillon, J. Talarmin, K. W. Muir, *J. Organomet. Chem.* **2001**, *627*, 67.
[44] M. R. DuBois, D. L. DuBois, M. C. VanDerveer, R. C. Haltiwanger, *Inorg. Chem.* **1981**, *20*, 3064.
[45] M. L. H. Green, J. D. Hubert, P. Mountford, *J. Chem. Soc. Dalton Trans.* **1990**, 3793.
[46] G. S. B. Adams, M. L. H. Green, *J. Chem. Soc. Dalton Trans.* **1981**, 353.
[47] F. Bottomley, L. Sutin, *Adv. Organomet. Chem.* **1988**, *28*, 339.
[48] C. Lin, T. Ren, E. J. Valente, J. D. Zubkovski, *J. Organomet. Chem.* **1999**, *579*, 114.
[49] C. Lin, J. D. Protasiewicz, T. Ren, *Inorg. Chem.* **1996**, *35*, 7455.
[50] U. Koelle, *New J. Chem.* **1992**, *16*, 157.
[51] E. Amouyal, in *Homogeneous Photocatalysis* (Ed.: M. Chanon), Wiley, **1997**, p. 263.
[52] H. Werner, W. Hofmann, R. Zolk, L. F. Dahl, J. Kocal, A. Kühn, *J. Organomet. Chem.* **1985**, *289*, 173.
[53] M. Maestri, N. Armaroli, V. Balzani, E. C. Constable, A. M. W. C. Thompson, *Inorg. Chem.* **1995**, *34*, 2759.
[54] G. Brauer, *Handbuch der Präparativen Anorganischen Chemie*, *Vol. 3*, 3rd ed., Ferdinand Enke, Stuttgart, **1981**.

[55] P. Wehman, G. C. Dol, E. R. Moorman, P. C. J. Kamer, P. W. N. M. van Leeuwen, *Organometallics* **1994**, *13*, 4856.
[56] M. Brookhart, B. Grant, A. F. Volpe, Jr., *Organometallics* **1992**, *11*, 3920.
[57] C. J. Harlan, A. J. Richard, S. U. Koschmieder, C. M. Nunn, *Polyhedron* **1990**, *9*, 669.
[58] H. Kiesele, *Anal. Chem.* **1980**, *52*, 2230.
[59] G. M. Sheldrick, SHELXS-97, Universität Göttingen, Göttingen (Germany), **1997**.
[60] G. M. Sheldrick, SHELXL-97, Universtität Göttingen, Göttingen (Germany), **1997**.

Received: August 9, 2002
Revised: February 28, 2003 [F4330]